

RESEARCH ARTICLE

# Storm types in Bangladesh: duration, intensity and area of intra-daily wet events

Vincent Moron<sup>1,2</sup> | Nachiketa Acharya<sup>3,4</sup> | S. M. Quamrul Hassan<sup>5</sup>

<sup>1</sup>Aix-Marseille University, CNRS, IRD, INRAE, Coll. de France, CEREGE, Aix en Provence, France

<sup>2</sup>IRI, Columbia University, Palisades, New York, USA

<sup>3</sup>Cooperative Institute for Research in Environmental Sciences (CIRES), University of Colorado Boulder, Boulder, Colorado, USA

<sup>4</sup>National Oceanic and Atmospheric Administration (NOAA) Physical Sciences Laboratory, Boulder, Colorado, USA

<sup>5</sup>Bangladesh Meteorological Department, Dhaka, Bangladesh

## Correspondence

Vincent Moron, Aix-Marseille University, CNRS, IRD, INRAE, Coll. de France, CEREGE, Aix en Provence, France.  
Email: [moron@cerege.fr](mailto:moron@cerege.fr)

## Abstract

We explore the characteristics of 96,190 wet events (WEs) defined as consecutive 3-hourly rainfall  $\geq 1$  mm/3 hr from a network of 34 stations across Bangladesh. Nearly 60% (5%) of WEs last  $\leq 3$  ( $\geq 15$ ) hr. The WEs are dynamically clustered into four “canonical” storm types (STs), mostly discretized by their duration, but also their mean and maximal intensity. While durations, total amounts and wet contiguous areas of WEs are positively related, their mean intensity is nearly independent of them. Approximately 60% of WEs are associated with ST#1, characterized by short and small WEs and very low rainfall amounts (usually  $<10$  mm),  $\sim 30\%$  of WEs are associated with either (ST#2) short/small WEs but with intense rainfall, probably mostly related to scattered thunderstorms or (ST#3) longer/larger WEs but with less intense rainfall. The last ST (ST#4) is rare ( $\sim 6\%$ ), related to very long durations and large wet areas and includes the wettest WEs. It is especially frequent over southeastern Bangladesh. ST#2–ST#4 contribute almost equally to the local-scale total amount of rainfall (27–29% each in mean) while ST#1, despite its individual low rainfall amount, still includes  $\sim 15\%$  of it. ST#2 (ST#4) is related to the highest probability of occurrence of 3-hourly (daily) extremes. ST#4 occurrence is the most impacted by synoptic Indian lows/depressions as well as the main modes of intra-seasonal variation, while ST#1 and ST#2 are also significantly impacted by intra-seasonal modes but in reverse manner than ST#4.

## KEYWORDS

3-hourly rainfall, clustering, predictability

## 1 | INTRODUCTION

Bangladesh is a flat deltaic country (Brammer, 2017) located on the northern edge of the Bay of Bengal (BoB) and is thus fully included in the domain of the Asian summer monsoon (Wang and LinHo, 2002; Gadgil,

2003). The seasonal changes of rainfall are mostly due to the meridional migration of the tropical convergence zone (TCZ) and its associated rainbelt, which are themselves mostly driven by the annual cycle of solar radiation combined with the large-scale land-sea contrast between Indian Ocean and Asia but also regional-scale

This is an open access article under the terms of the [Creative Commons Attribution](https://creativecommons.org/licenses/by/4.0/) License, which permits use, distribution and reproduction in any medium, provided the original work is properly cited.

© 2022 The Authors. *International Journal of Climatology* published by John Wiley & Sons Ltd on behalf of Royal Meteorological Society.

orography (Gadgil, 2003). Even if Bangladesh is considered to be part of the Indian monsoon system (Wang and LinHo, 2002), the monsoon season starts earlier over Bangladesh than over the mainland India (Ahmed and Karmakar, 1993) and covers roughly the period from May to October (Islam *et al.*, 2005a; Islam and Uyeda, 2007; Shahid and Khairulmaini, 2009; Montes *et al.*, 2021).

Bangladesh represents one of the wettest sectors (1,500–4,500 mm-season<sup>-1</sup>) of the whole Asian boreal summer monsoon domain with western Indian Ghats, Indian Assam, coastal Myanmar and southern Indochina (Wang and LinHo, 2002). The large rainfall amount received usually in only 6 months, with a peak in June–August, is induced by the multiscale interaction between various fixed and transient factors. It includes the location of the country windward to the usual southerly moist and warm low level flow from BoB, the cyclonic curvature of this flow due to its veering towards the low pressure area over northwestern India and the Gangetic plain, as well as the orographic forcing due to Assam hills, just northeast of Bangladesh, which includes one of the rainiest location on the Earth (Cherrapunji) (Basher *et al.*, 2018), and Chittagong Hill Tracts running along the Myanmar's border, southeast of the country. As a consequence, seasonal rainfall is relatively low (~1,300–1,500 mm) in the central-western parts of the country and peaks >4,000 mm near the northeastern and southeastern borders (Shahid and Khairulmaini, 2009; Shahid, 2011).

Due to its low altitude, complex and dense river system and the usually large and concentrated rainfall, Bangladesh is very vulnerable to climatic risks, mostly extreme rainfall and flooding and associated landslides as soon as slopes exist, but also sea surges associated with cyclonic systems coming from BoB (Dastagir, 2015). The rainfall variability may be linked, as elsewhere over the whole Asian summer monsoon domain, to the interactions between various drivers at synoptic (including lows and depression in or close to TCZ), intra-seasonal (including 30–60 day [Singh *et al.*, 1992] and quasi-biweekly (QBW) [Kikuchi and Wang, 2009] modes of variation well involved in the active-break cycle of the boreal summer monsoon) as well as interannual (as El Niño Southern Oscillation (ENSO), Indian Ocean Dipole) drivers.

The rainfall variability from the daily time scale has already been explored. Shahid (2011) analysed extreme rainfall indices from a network of nine stations in the 1958–2007 period. He emphasized an increase of heavy rainy days, mostly over northwestern Bangladesh, especially for the pre-monsoon period. In contrast, Basher *et al.* (2018) found a consistent negative trend in the pre-monsoon and monsoon extreme rainfall over the wet northeastern Bangladesh from a network of seven

stations in the 1984–2010 period. It somehow contrasts with the study of Rimi *et al.* (2019) concluding that anthropogenic climate change doubled the likelihood of an extreme pre-monsoon event (a 6-day event accounting for 225 mm of rainfall in March 2017) over northeastern Bangladesh. Lastly, Islam *et al.* (2020) showed also contrasted decreasing and increasing trends in the frequency of various daily amounts from  $\leq 5$  to  $\geq 35$  mm from a network of 23 stations in the 1975–2017 period. They also indicated that the spatial coherence of these trends is weak at the country scale. The lack of consistency about the polarity of trends and spatial coherence across the country may be due to different time periods and spatial samplings, but may also be a true sign of weak and insignificant trends from the 1950s.

Use of intra-daily or daily rainfall may lead to different outputs when extreme rainfall is analysed (Barbero *et al.*, 2017). It is also rather well established that wet events (WEs), simply defined as consecutive wet hours recorded at a given rain gauge, last usually far less than a full day at least across the tropical continents (Ricciardulli and Sardeshmukh, 2002; Trenberth *et al.*, 2017; Zhang and Wang, 2021). A given daily amount may then combine two potentially different pieces of information, that is, the duration of WE and the mean intensity of rainfall at the intra-daily time scale. For example, a daily amount of 50 mm may be a relatively long and moderately intense event (as 10 consecutive hours with a 5 mm-hr<sup>-1</sup> mean intensity) or a short intense thunderstorm lasting less than 1 hr (so with a “mean” intensity of 50 mm-hr<sup>-1</sup> with an hourly resolution). The social and environmental consequences of both events, identical at the daily time scale, as well as their atmospheric drivers may be fairly or even radically different. For example, the risk of flash flood is clearly increased in the second versus the first case. These potential differences may also be on their level and source of predictability. This is why it is important to consider intra-daily rainfall records.

The space–time variability of sub-daily rainfall is here explored on an original network of 3-hourly rainfall recorded at 34 rain gauges Bangladesh Meteorological Department (BMD) from 1998 to 2019. Section 2 presents the data while Section 3 analyses the results. A discussion and conclusion (Section 4) close the paper.

## 2 | DATA AND METHODOLOGY

### 2.1 | 3-Hourly rainfall data from ground observation

3-Hourly rainfall has been extracted from the synoptic station maintained by BMD and used to define the WEs,

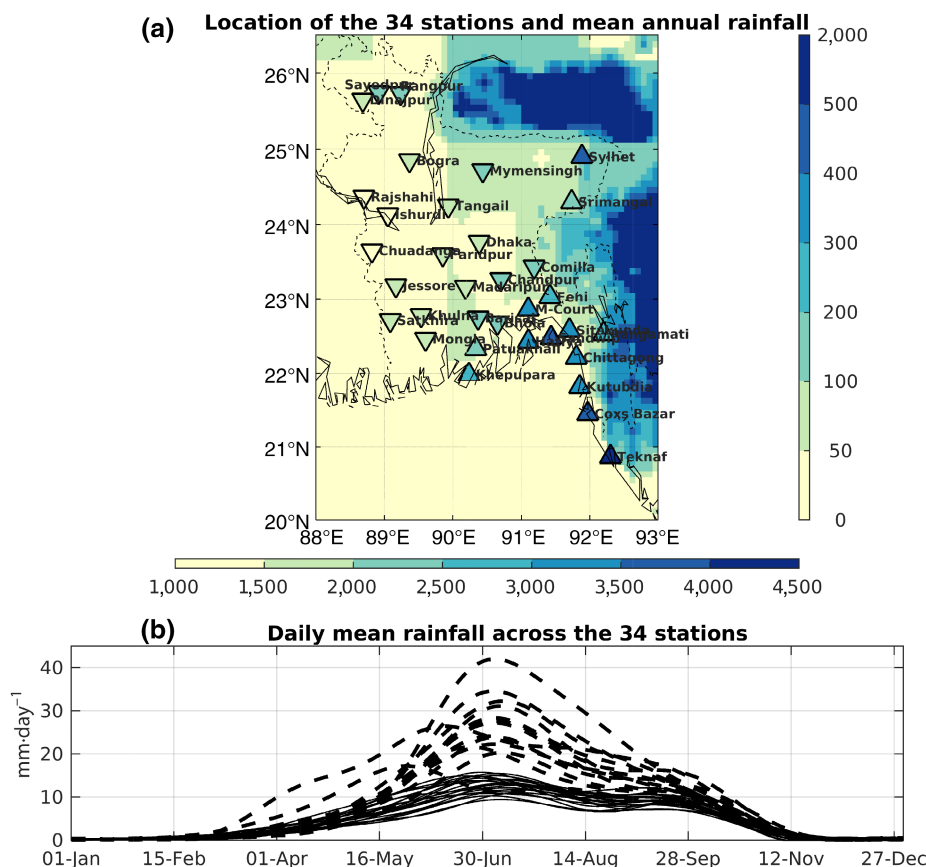


**FIGURE 1** (a) Location of the 34 stations superimposed over the topography (shadings in metres above sea level, right legend) and with the mean annual rainfall (in millimetres, bottom legend) coded as upward and downward triangles. (b) Daily mean rainfall across the 34 stations averaged over the 22 years and low-pass filtered with a Butterworth's recursive filter with a cut-off at 1/60 cycle-per-day. The dashed lines show the stations with an upward triangle in (a) and the full lines show the stations with a downward triangle in (a) [Colour figure can be viewed at [wileyonlinelibrary.com](http://wileyonlinelibrary.com)]

which are simply consecutive 3-hourly slots receiving at least 1 mm. These stations are maintained by following WMO's standard. For 31 out of the 34 stations shown in Figure 1a, there are very few missing entries (maximum = fifteen 3-hr slots over the whole available period). A full year of 3-hourly data is missing at Sitakunda (2002), Patuakhali (2000) and Hatiya (2003). In total, the amount of missing entries equals 0.4%. Missing entries are not filled and only available data are used in the following statistical analyses. We cannot totally exclude that some missing entries are filled by zeros at unknown temporal and spatial locations, but we believe that these possible errors do not significantly impact our results, due to our focus on the local-scale sequences of consecutive 3-hourly wet periods. Any possible extra sequence of zeros is, by definition, not included in this sample. Lastly, our maps of results (Figures 2, 5, 8, 9, 12 and 13) do not show any spurious spatial pattern or very dissimilar behaviour between close rain gauges. We conclude that this network is adequate for our purpose. Figure 1a shows the location of the 34 synoptic stations superimposed on the topography. Bangladesh is a flat country with several hills close to the northeastern and eastern borders, peaking near 1,000 m in the Chittagong Hill Tracts close to Myanmar's border. Figure 1b shows that ~80% of the annual rainfall occurs in May–October with a peak usually around late June to early July. Two stations (Sylhet and Srimangal) located in the northeast of the

country (Figure 1a) show a slightly different annual cycle, with rainfall starting and peaking earlier than elsewhere. Lastly, the stations with a maximum daily mean rainfall  $\geq 20 \text{ mm day}^{-1}$  sometimes in June–September are mostly located in the southeast of the country, approximately south-east of a line stretched from Hatiya to M-Court and Feni (Figure 1a) and in the extreme southern part of the delta (i.e., Khepupara and Patuakhali, Figure 1a), and lastly at the station of Sylhet. The remaining stations, covering most of the country, never reach this threshold (Figure 1b) and show a very similar annual cycle either in amplitude or in phase (blue dots in Figure 1a and blue lines in Figure 1b).

So in summary, most of Bangladesh receives usually 1,500–2,500 mm of rainfall mostly in May–October, in relation to the boreal summer monsoon with a very consistent amplitude and phase. Rainfall notably increases towards the southeast of the country, without a large change in phase while two stations in the northeast show a longer rainfall season mostly due to an earlier start than in the rest of the country.

## 2.2 | Satellite rainfall products

We extracted the 30-min IMERG TMPA data (final release, Huffman *et al.*, 2017, 2019, 2020) on the native  $0.1^\circ$  grid from June 2000 to December 2019. In a recent

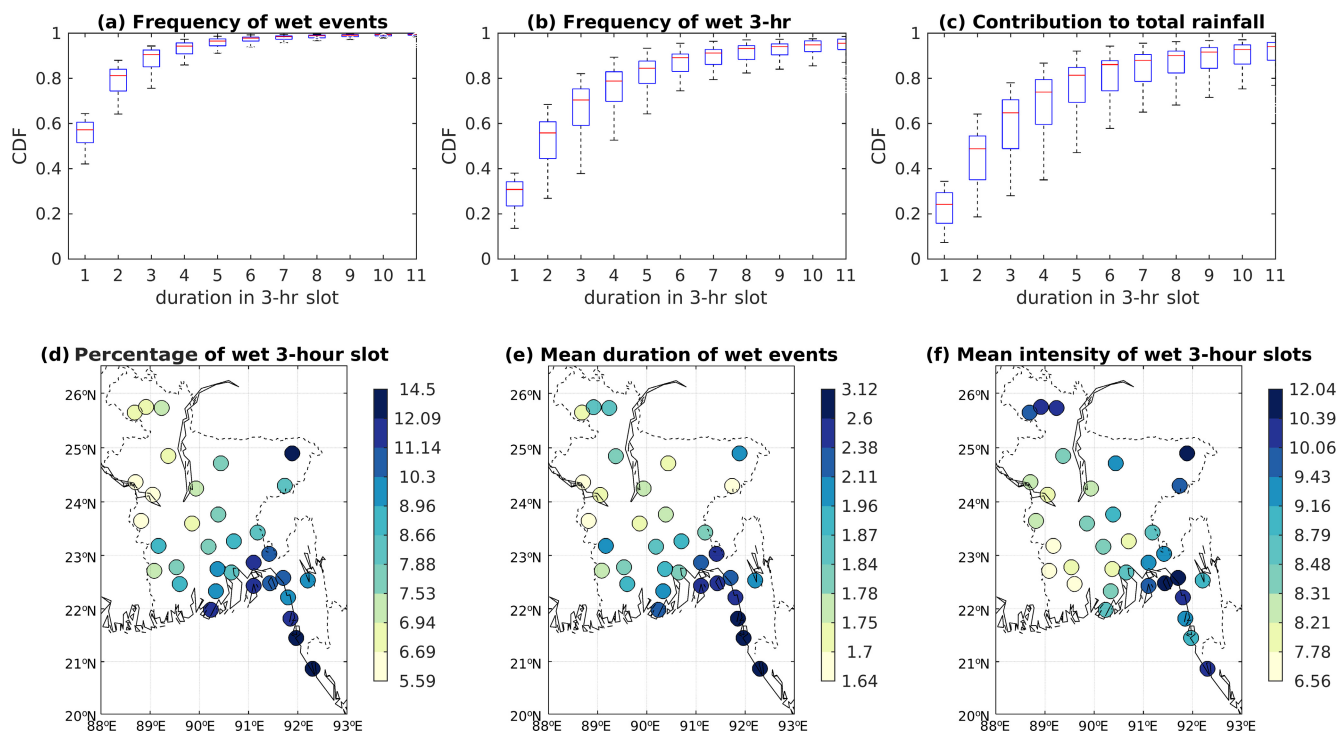


**FIGURE 2** Cumulative distribution function of (a) the wet events (defined from consecutive wet 3-hr slots  $\geq 1$  mm), (b) the wet 3-hr slots and (c) the contribution to total rainfall amount vs their duration (in 3-hourly slots) computed independently on each station (and all available periods). For the three variables, the boxplots (upper and lower limits of the box are 25th and 75th percentiles while the red line is the median) are shown for the 34 stations and all durations from 3 to 33 consecutive hours. (d) Mean frequency (in percentage of the available period) of the wet 3-hr slots, (e) mean duration of wet events (in 3-hr slots) and (f) mean intensity of wet slots (as the mean rainfall in mm received during the wet 3-hr slots) [Colour figure can be viewed at [wileyonlinelibrary.com](http://wileyonlinelibrary.com)]

study, Montes *et al.* (2021) compared various satellite rainfall products (IMERG, CHIRPS, PERSIANN-CDR, CMORPH) with BMD's rain gauge for intense rainfall on a daily time scale. They found that IMERG showed the best performance overall, in particular the high intense rainfall ( $>20 \text{ mm} \cdot \text{day}^{-1}$ ) events. Islam (2018) analysed 3-hourly amounts produced by various satellite products (including IMERG calibrated or not by rain gauge) in the 2014–2016 period. He revealed that all products are doing well in detecting the occurrence of rainfall, but are not so good in estimating the amount of rainfall. Ahmed *et al.* (2021) also recently showed that IMERG reproduces rather well than the diurnal cycle of rainfall across Bangladesh, except for the overestimation of the amplitude of diurnal variability in the pre-monsoon season for the 2015–2019 period.

IMERG is mostly used here to analyse the spatial extent of WEs defined from the network of the 34 rain gauges. The dates and locations of the WEs are defined from BMD's network and then, the total rainfall amount for each of the WEs is summed on a  $10^\circ \times 10^\circ$  grid centred on the target BMD station. The choice of this area is firstly constrained by the length scale of the largest rain-bearing system operating over Bangladesh, that is, low

pressure systems (LPS) including the tropical cyclones. It is usually assumed that most of the LPS related to Indian monsoon forms over the head of the BoB, move northwestward across the Gangetic plain, have a life cycle of 3–6 days and an horizontal length scale of about 1,000–2,000 km (i.e., Mooley, 1973; Godbole, 1977; Sikka, 1978). The rainfall is usually organized in 50–150 km wide bands rotating around the centre of the LPS. For example, Mooley (1973) studied the daily rainfall associated with LPS within 500 km of 24-hr mean position of depression centre. We may assume that considering a 3-hourly instead of a daily time scale reduces, at least slightly, the contiguous wet areas. Previous studies focusing on and around Bangladesh and using a time scale less than a day show even reduced spatial scales. For example, Rafiuddin *et al.* (2007, 2010) indicated that the average horizontal length of precipitation systems defined from BMD weather radar (in April–September in 2000–2005) ranges from 184–185 km, for “arc” and “line” to 286 km for “scattered” patterns respectively. So a  $10^\circ \times 10^\circ$  grid centred on each station recording a WE appears to be a reasonable choice to include all contiguous wet areas associated with the largest possible rain-bearing systems in this



tropical sector. We also made some comparison between BMD total rainfall amount received for each WE and what is recorded in IMERG at the closest co-located grid-point for the same WE.

## 2.3 | Daily outgoing longwave radiation

Daily outgoing longwave radiation (OLR) has been extracted from NOAA website in the 1998–2019 period at an horizontal resolution of  $1^\circ$  (Liebmann and Smith, 1996). We used OLR data here to define the intra-seasonal modes of variation.

## 2.4 | Best tracks of LPS

Best tracks of LPS (Goswami *et al.*, 2003) travelling around India and diagnosed by the Indian Meteorological Department (IMD) have been extracted from [https://rsmcnewdelhi.imd.gov.in/report.php?internal\\_menu=MzM=](https://rsmcnewdelhi.imd.gov.in/report.php?internal_menu=MzM=) in the 1998–2019 period. The dataset provides 3-hourly time coordinates, longitude/latitude coordinates, central pressure, wind gusts and categories of each LPS which are also sometimes named. Note that these LPS are usually larger than the ones detected specifically over and around Bangladesh by Hatsuzuka *et al.* (2014) and Hatsuzuka and Fujinami (2017). When two locations for the same LPS are provided with a time step above 3 hr, we interpolate the location at each intermediate 3 hr slot between two available ones. When two events occur at the same date, we consider only the closest to the BMD network using the spatial average across the 34 stations. The categories for the available 6,679 three-hourly time steps between 1998 and 2019 are almost always (except two cases categorized as “low” and one case not categorized) at least “depression.” We merge the categories “depression” (maximum sustained wind 17–27 knots, i.e.,  $31\text{--}49\text{ km}\cdot\text{h}^{-1}$ ) and “deep depression” (maximum sustained wind 28–33 knots, i.e.,  $50\text{--}61\text{ km}\cdot\text{h}^{-1}$ ) into a single “depression” category and all other “cyclonic storms” (maximum sustained wind  $\geq 34$  knots, i.e.,  $\geq 62\text{ km}\cdot\text{h}^{-1}$ ) categories as a single “cyclone” category (Sabeerali *et al.*, 2022).

## 2.5 | Methodology

We started from the analysis of the local-scale WEs defined independently on each station of the network. A total of 96,190 WEs (i.e., roughly 129 WEs in mean per year and station) were obtained. We derived the following characteristics for each WE: duration from

its start to its end, total amount of rainfall, maximum intensity (in  $\text{mm}/3\text{ hr}$  = highest 3-hourly rainfall amount in mm during each WE) and mean intensity (in  $\text{mm}/3\text{ hr}$  = total amount in mm of each WE divided by its duration).

The set of 96,190 WEs is then clustered using a dynamical  $k$ -means (Diday and Simon, 1976) into a parsimonious set of canonical temporal patterns, referred to as local-scale storm types (STs) following the methodology of Moron *et al.* (2021). STs define simply the local temporal variations of the 3-hourly rainfall during any WE from its start. As a first guess, STs may be discretized by, at least, their durations and total amounts. We considered the 3-hourly rainfall amounts of the eight first 3-hr periods of any WE (98% of all WEs last less or equal to 24 consecutive hours). If it does rain less than 1 mm, the corresponding 3-hourly amount is set to zero. To reduce the skewness, the square root of 3-hourly amounts was computed and the eight 3-hourly amounts were standardized against the 3-hourly means from the start of WEs.

The matrix of 96,190 rows and 8 columns is then subjected to a  $k$ -means clustering with an empirical orthogonal function (EOF) pre-processing. We used 1,000 replicates starting from random initial seeds for each clustering solution from  $k = 2$  to  $k = 10$ . The  $k$ -means clusters localize high concentrations of points in the phase subspace spanned by the leading EOFs explaining 90% of the total variance. Their centroids are given by averaging the 3-hourly rainfall anomalies over all WEs that belong to a given cluster and they define each distinct ST. The  $k$ -means clustering needs to first choose the number of clusters (i.e., the value of  $k$  between 2 and 10 here). First of all, there is no universal score to define the optimal number of clusters, as soon as real world data are considered. Climate variations are inherently continuous and clustering should be rather understood as a compact description of complex variations rather than delineating discrete and well-separated groups. The classifiability index (CI, Michelangeli *et al.*, 1995; Roller *et al.*, 2016) computes basically the sensitivity of the clustering to the initialization of random seeds. From that point of view, a “perfect” classification corresponds to a CI of 1, meaning that the final clustering does not depend at all on initialization of clusters (i.e., the 1,000 replicates with different initializations lead to the same final clustering). We also used another score measuring the fraction of variance of WEs characteristics explained by the clustering. The relative fraction of variance increases as the number of clusters grows but this is almost fully expected. A good value of  $k$  may be one where the increase of explained variance is relatively large against  $k - 1$  and relatively low against  $k + 1$ .

### 3 | RESULTS

#### 3.1 | WEs and climatological rainfall

Figure 2a–c shows some climatological features of the 96,190 WEs. We restricted our displaying to WEs lasting less or equal to 33 hr (average duration of WEs = 2.05 3-hourly slots), including 99% of all WEs (the longest WE lasts a week). As shown elsewhere (Moron *et al.*, 2021), there are a lot of short WEs and their relative frequencies (Figure 2a) that tend to decrease quickly as their duration grows. Obviously, the relationship is less steep when the frequency of wet 3-hr is considered (Figure 2b) since the simple frequency of WEs is then weighed by their length. Nevertheless, around 90% of wet 3-hr are included in WEs lasting less or equal than a full day (Figure 2b) similarly to what is found in India (Deshpande *et al.*, 2012; Moron *et al.*, 2021). The cumulative distribution function of the contribution of total rainfall shows again an exponential increase (Figure 2c) with around 50% (respectively 80%) of total rainfall due to WEs lasting less or equal than 6 (respectively 18) hr.

Figure 2d–f explores the climatological features of frequency of wet 3-hr slots, mean duration of WEs and mean intensity of rainfall in 3-hr slots. It is interesting to compare these maps to the mean rainfall amounts shown in Figure 1a. As demonstrated elsewhere (i.e., Moron *et al.*, 2007), the spatial variations of total amount are more related to frequency (Figure 2d) than with intensity (Figure 2f) with correlations respectively equal to .93 and .69 (correlation between frequency and intensity equals .39). The mean duration (Figure 2e) is tightly related to the frequency ( $r = .88$ ) for a simple reason, which is the fact that increasing the frequency of wet 3-hr slots increases, by definition, their temporal aggregation, just by reducing the inter-event distance. Of course, there are also meteorological reasons since mesoscale convective complexes and larger/longer rain-bearing systems as tropical lows or depressions may increase the duration of WEs.

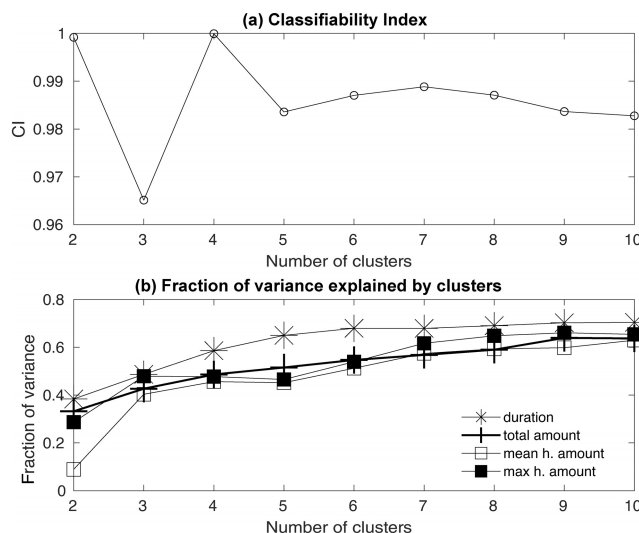
#### 3.2 | Definition of the optimal number of clusters

Figure 3 shows some metrics used to choose the final number of clusters. CI (Figure 3a) shows maxima at  $k = 2$  and  $k = 4$  but the other solutions of  $k$  are not so different from the optimal value of 1. The fraction of variance explained by the 2–10 clusters (Figure 3b) increases strongly between  $k = 2$  and  $k = 3$ , but thereafter, no systematic flat or jump appears at the same value of  $k$  for the different WE characteristics. For duration, the main

flat occurs at  $k = 6$  while for total amount, it occurs at  $k = 9$ . For mean intensity, the main flat occurs at  $k = 4$  with even a small decrease of the explained variance at  $k = 5$ . As the mean intensity conveys an almost independent information relative to both duration and total amount, as shown in Figure 4, we retain  $k = 4$  as the most parsimonious solution offering a sufficient discretization of all variables considered in Figure 3b.

#### 3.3 | Climatological features of the STs

Figure 4a shows that duration is tightly related to the total quantity in WEs ( $r = .78$ ). Three STs out of four (except ST#2) are primarily discriminated by the duration of the WEs and total amount of rainfall since they are broadly aligned on the linear fit between both variables (Figure 4a). ST#1 ( $n = 58,499$  WEs) is related to very small amounts and durations (i.e., ST#1 includes more than 90% of all WEs receiving less than 10 mm of rainfall). ST#2 ( $n = 16,516$  WEs) and ST#3 ( $n = 15,575$  WEs) receive similar amount of rainfall but ST#2 is far shorter than ST#3 (Figure 4a). ST#4 ( $n = 5,600$  WEs) receives a larger amount during a longer duration. The discrimination of mean (Figure 4b) and maximum (Figure 4c) intensity by STs is subtil. First, mean intensity and duration (Figure 4b) are basically independent (less than 1.5% of common variance) and ST#2 is now the more intense



**FIGURE 3** (a) Classifiability index (from Michelangeli *et al.*, 1995 modified by Roller *et al.*, 2016) versus the number of clusters. A value of 1 means that clustering is fully insensitive to the initial random seeds. (b) Fraction of variance of duration, total amount, mean intensity and maximum intensity explained by the 2–10 clusters (given by the ratio between the inter-cluster vs. total variance). All values are significant at the 99% level according to Fisher's  $F$ -test

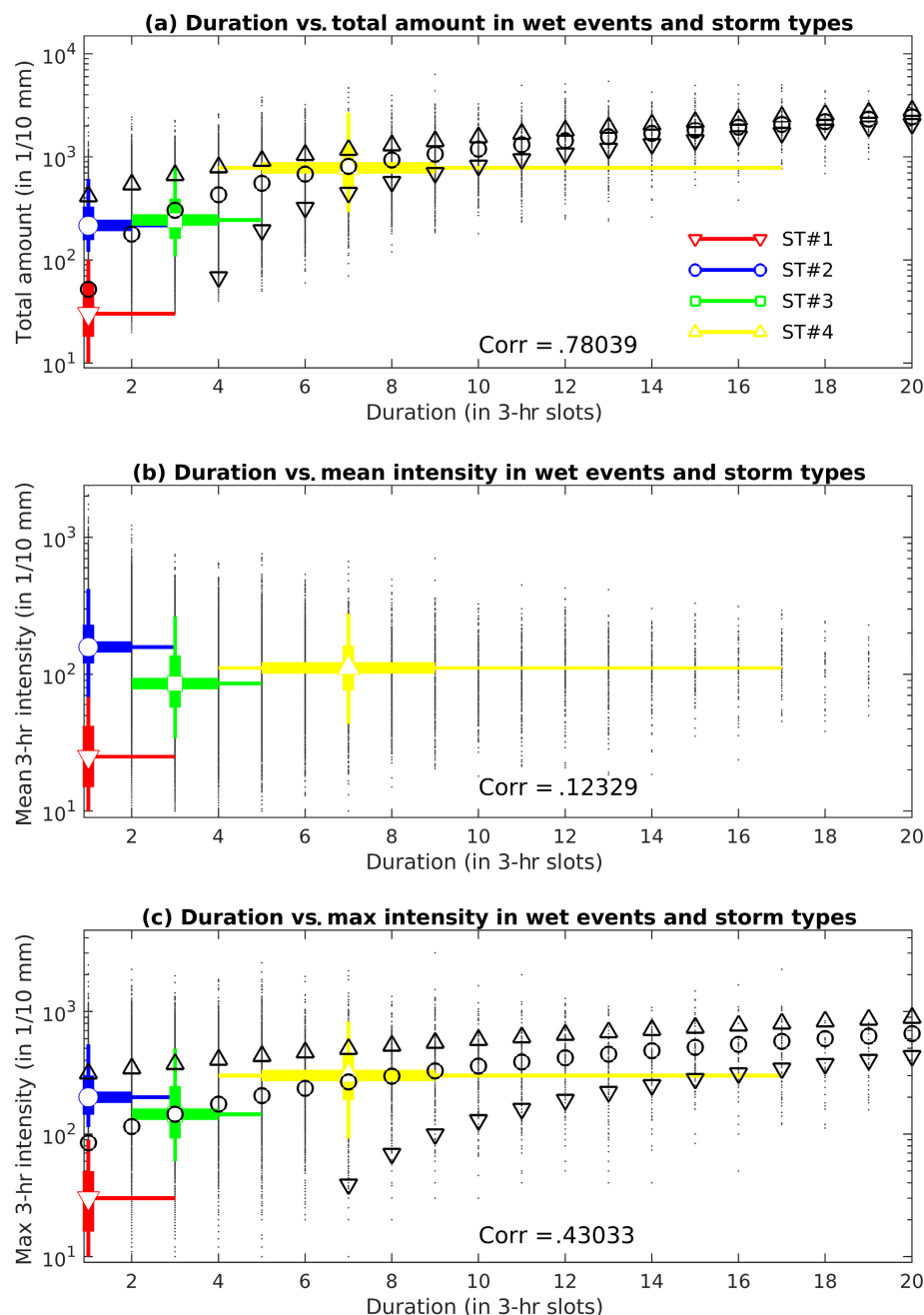


**FIGURE 4** Scatter plot (grey dots) of the duration (in 3-hr slots) of the 96,190 wet events in abscissa versus (a) their total rainfall (in 1/10 mm), (b) their mean intensity (in 1/10 mm in 3-hr slots) and (c) their maximum intensity (in 1/10 mm in 3-hr slots) in ordinates. The median (large markers) with the 25th–75th (large lines) and 5th–95th (thin lines) percentiles are superimposed for the four STs defined in panel (a). The black circles in panels (a) and (c) represent the linear fit (computed from all wet events) between duration and the variables shown on the ordinate of each panel with the upward and downward black triangles showing the two-sided 90% interval of confidence. Due to Y-axis log scale, negative values of the lower confidence bound are not shown for short durations. In panel (b), the linear fit is not shown since the linear correlation between duration and mean intensity explains less than 2% of the total covariance [Colour figure can be viewed at [wileyonlinelibrary.com](http://wileyonlinelibrary.com)]

ST in mean, slightly before ST#4 and ST#3 (Figure 4b). ST#2 is then related to short but intense mean rainfall, while ST#3 and especially ST#4 are associated with longer WEs with usually moderate mean intensity, at least in relative terms. ST#1 is related to very low mean intensity (Figure 4b). Maximum 3-hourly intensity (Figure 4c) is again related to duration as for the total rainfall received during WEs. It could be interpreted as the fact that a longer duration leads to a higher probability to get a large 3-hourly amount. It is rather expected if we assume that near-instantaneous rainfall, nonetheless not well resolved by a 3-hourly time step, follows a quasi-exponential distribution. Now, ST#4 leads to the

maximum 3-hourly amount slightly behind ST#2 and then ST#3, ST#1 being again related to a very small maximum 3-hourly amount (Figure 4c).

So overall, these results are consistent with those obtained over India (Moron *et al.*, 2021), even if the temporal resolution is different (3-hourly vs. hourly). The most frequent ST#1, by far, is related to nominal amounts, short duration and low mean and maximum intensities. Then, ST#2 represents short but intense events while ST#3 receives a similar amount of rainfall, but distributed over a longer period, thus with a lower mean intensity than ST#2. ST#4, which is rare (i.e., 10 times less frequent than ST#1), receives the largest

amount during the longest durations, with some very high peak intensity even if the mean intensity is lower than for ST#2.

Figure 5 shows the relative frequencies of each ST across space and across the year. The spatial variations of STs#1–3 are relatively small ( $CV < 15\%$ ) while the pattern correlations of ST#1, ST#3 and ST#4 relative frequencies with the mean annual rainfall shown in Figure 1a are very high (respectively  $-.88$ ,  $.90$  and  $.87$  for ST#1, ST#3 and ST#4). So driest (wettest) parts of Bangladesh are related with relatively more (less) ST#1 and less (more) ST#3 and ST#4. ST#2 shows a slightly different pattern with a pattern correlation with annual mean (Figure 1a) equal to  $-.49$ . The gradient is now between north and south of Bangladesh rather than between the central and northern part and the extreme southeast (+Sylhet).

In time, the absolute frequency of all STs (black line in Figure 5e) conveys basically, and logically, the same information as the mean rainfall shown in Figure 1b. But, we can also notice that ST#2 is especially relatively frequent before and around the onset date from mid-March to mid-June, during the pre-monsoon season (Figure 5e). This relative maximum fits well with Rafiuddin *et al.* (2007, 2010) and Islam *et al.* (2005b) who showed that small and fast (i.e., short at a fixed location as ST#2) precipitation systems are especially frequent during the pre-monsoon season. The largest relative frequency of the longest ST#4 occurs near the annual rainfall peak but also after the rainy season in November (Figure 5e). This post-monsoon relative maximum fits well with the second cyclonic season over the BoB (Sattar and Cheung, 2019), even if the absolute frequency of all STs is then far lower than that during the monsoon season (Figure 5e).

Note that the contribution of each ST to the total rainfall (not shown) is highly related to the map of frequency (Figure 5a–d) for ST#1 (patt. corr. =  $.92$ , average contribution =  $15\%$ ), ST#2 (patt. corr. =  $.84$ , average contribution =  $27.5\%$ ) and ST#4 (patt. corr. =  $.98$ , average contribution =  $29.5\%$ ). ST#3 shows a different pattern (patt. corr. =  $.05$ ), with maxima over northern Bangladesh and southern Delta and minima over western-central and extreme southeastern parts of the country, but the average contribution to total rainfall ( $28\%$ ) is the least variable across the country ( $CV = 13\%$  vs.  $>25\%$  for the other three STs).

A last property of the STs is the continuous wet area around each target station to give an empirical estimate of the spatial scale and thus the most probable meteorological rain-bearing process associated with each ST (Orlanski, 1975; Moron *et al.*, 2021). In Figure 6, we evaluated the mean IMERG rainfall for each WE belonging

to the STs for a  $10^\circ \times 10^\circ$  square centred on the co-located IMERG grid-point with the 34 BMD stations. We also showed the scatter plot of the total rainfall received at BMD and its co-located IMERG grid-points. As already seen for India (Moron *et al.*, 2021), the nominal and short ST#1 and short but intense ST#2 are less accurately estimated than the longest events ST#3 and ST#4. The bias is especially negative in ST2 (almost 50% of the observed amounts) and clearly better in ST#3 and ST#4 even if IMERG still usually underestimated the total rainfall received at the BMD rain gauges. The wet area is small in ST#1 (Figure 6a), but also in ST#2 (Figure 6c) and larger in ST#3 (Figure 6e) and especially in ST#4 (Figure 6g). Note that the stretched relative maximum elongated southeastward from the target may be related with the shape of the country and the usual highest amount observed over the southeast, windward of the Chittagong Hill Tracts (Figure 1a). Independent from the event and in association with the spatial sampling of the rain gauges, it tends to rain more southeast of any  $10^\circ \times 10^\circ$  window centred on one of the 34 rain gauges. This anomaly is very weak for ST#2 (Figure 6c) and strongest for ST#4 (Figure 6g).

Figure 7 explores the relationships between wet area, duration, total amount and mean intensity using a similar illustration as Figure 4. We selected here only the observed WEs receiving at least 10 mm of rainfall at the BMD rain gauge strongly reducing the sample of ST#1 ( $n = 3,914$ ) but considering 95–100% of all remaining three STs. Note that 73.5, 63, 45 and 17% of the STs#1–4 receiving at least 10 mm at the BMD rain gauges are associated with a zero surface receiving at least 10 mm at the target. So, we considered here only the WEs receiving at least 10 mm at the BMD rain gauge and at its collocated IMERG grid-points. The sample size reduces to respectively 1,047 ST#1, 6,122 ST#2, 8,424 ST#3 and 4,662 ST#4 (total  $n = 20,255$ ). ST#2 now exhibits the smallest surfaces, almost as equal as those related to ST#1, while ST#3 and especially ST#4 are far larger (Figure 7). Figure 7a shows a large correlation between duration and surface of wet areas. It could be interpreted as the fact that over land, a longer WEs (especially ST#4 and secondary ST#3 here) may have more probability to propagate in any direction, thus wetting a larger surface and/or (b) any meteorological event (meso-scale complexes, depression, cyclone, wave, etc.) able to sustain convection for more than few hours are usually associated with larger wet surface than unitary cumuliform cloud. The relationship between surface of wet areas and total amount received at the BMD rain gauge (Figure 7b) is noisier than previous ones, but there is still a positive near-linear link between both variables. Now, ST#2, ST#3 and ST#4 are almost aligned



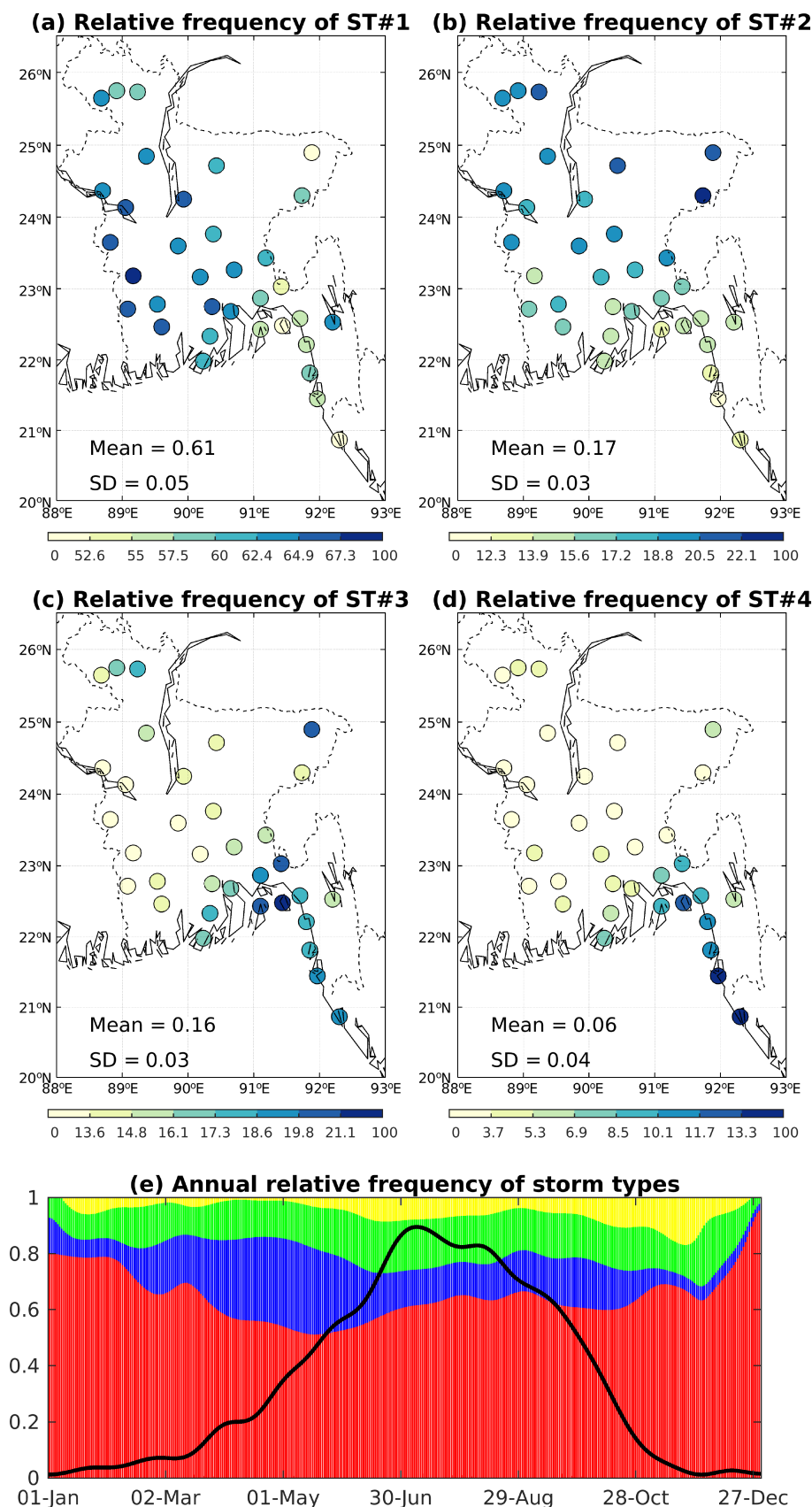


**FIGURE 5** (a–d) Relative frequency of storm types (ST) #1–#4 with spatial average and standard deviation (SD) across the 34 stations shown in the lower left corner of each map. (e) Daily relative frequency of STs (displayed with the same colour as in Figure 4). The black line is the relative daily frequency of all STs considered together across the 34 stations (a value of 1 means that all stations receive at least 1 mm/3 hr all years. All time series in panel (e) are daily averages low pass filtered with a cut-off at 1/30 cycle-per-day [Colour figure can be viewed at [wileyonlinelibrary.com](http://wileyonlinelibrary.com)]

on the linear fit while ST#1 appears to be far below. Note that using IMERG total rainfall (instead of the BMD one) at the co-located BMD rain gauge location

leads to the same correlation coefficient. Figure 7c shows that mean intensity is not really related to the surface of the wet area. Note that maximum intensity

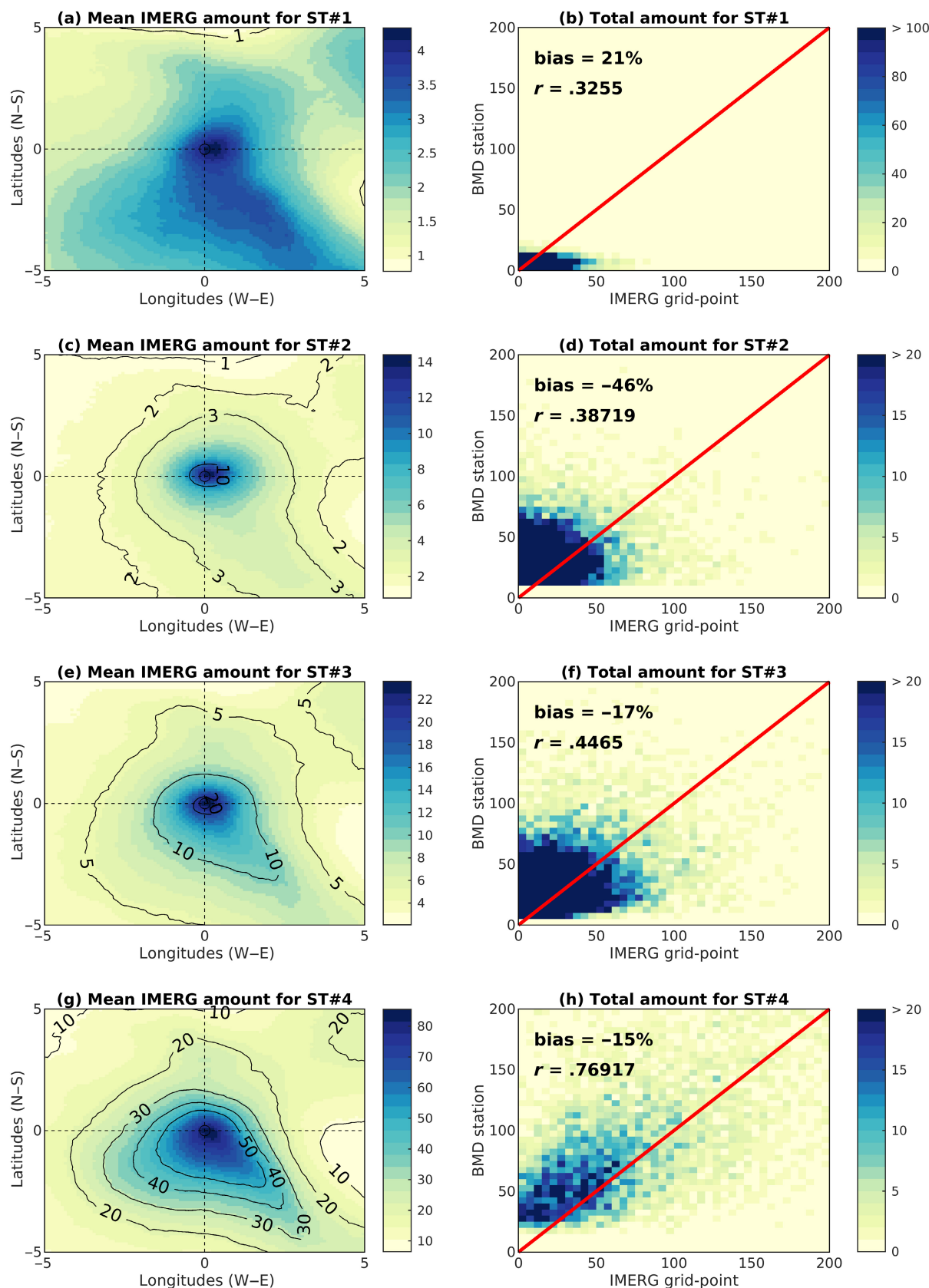


**FIGURE 6** IMERG mean total rainfall amount for (a,c,e,g) storm types (ST) #1–#4 in mm. Contours are superimposed on colours at 1, 2, 3, 5, 10, 20, 30, 40 and 50 mm. (b,d,f,h) Binned frequencies (with a step of 10 mm) of BMD and IMERG total rainfall amount (in mm) during observed WEs belonging to a ST received at the target (= (0,0) location of left panels) co-located with the BMD rain gauges locations [Colour figure can be viewed at [wileyonlinelibrary.com](http://wileyonlinelibrary.com)]

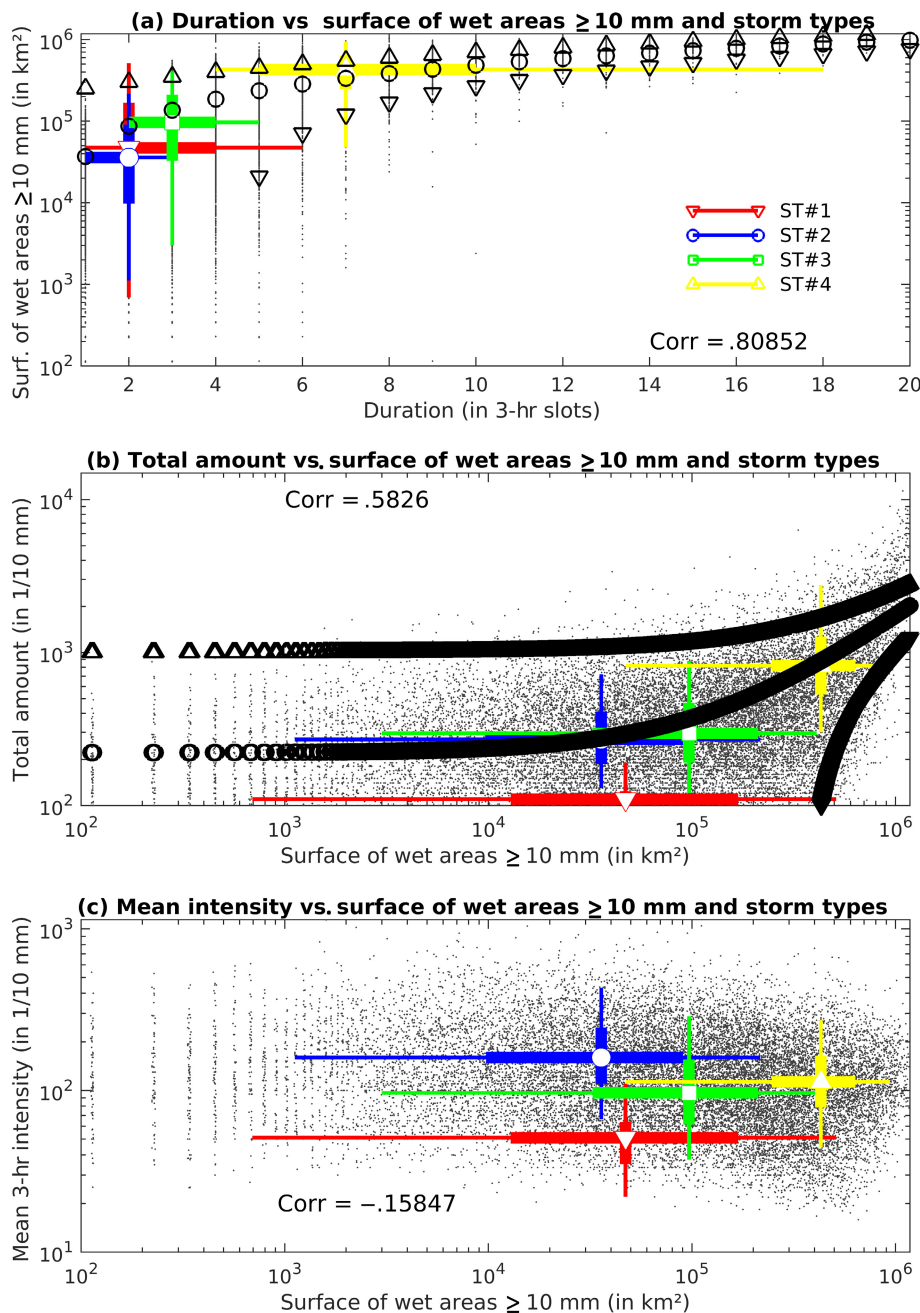


**FIGURE 7** Same as Figure 4, except between the surface of IMERG wet area (in  $\text{km}^2$ ) receiving at least 10 mm and (a) duration of wet events (WE) (in 3-hr slots), (b) total amounts (in 1/10 mm) and (c) mean intensity (in 1/10 mm per 3 hr) at the target BMD rain gauges. The sample is here reduced to WEs receiving at least 10 mm at the BMD rain gauge and at the co-located IMERG grid-points. Note that the linear fit line is not indicated on panel (c) because the common variance is  $<2\%$  [Colour figure can be viewed at [wileyonlinelibrary.com](http://wileyonlinelibrary.com)]

shares a low correlation of coefficient ( $r = .19$ ) with the surface of the wet area (not shown).

### 3.4 | STs and modulation of country and local rainfall 3-hourly and daily extremes

We define four categories of daily and 3-hourly rainfall from the BMD definition to delineate five classes of light, moderate, moderate-heavy, heavy and very heavy daily rainfall which are respectively 9.65, 22.35, 44.2 and

89 mm. These values correspond respectively to percentiles 0.47, 0.70, 0.86 and 0.96 in our network when only daily values  $\geq 1$  mm recorded at the 34 stations are considered. Then, the corresponding raw 3-hourly rainfall  $\geq 1$  mm for the same percentiles equal respectively 4, 9, 18.2 and 38.5 mm. Note that the same percentiles for the WEs equal respectively 6.4, 16.3, 35 and 79 mm, thus between the raw values at the 3-hourly and daily time scales, consistent with the mean duration of all WEs. The relative risk ratio (RR) is then computed for 3-hourly and daily rainfall exceeding the four thresholds defined above

for each ST. The upper row of Figures 8 and 9 considers the total RR independently on stations, that is counting the 3-hourly and daily rainfall “extremes” above the four thresholds defined above across the 34 stations together, while the lower three rows show the local RR computed at each station for ST#2, ST#3 and ST#4. The corresponding maps are not shown for ST#1 since the total and local RRs are almost always close to zero. For example, while ST#1 includes roughly 61% of all WEs, only 10% of the WEs receiving  $\geq 9.65$  mm (i.e., corresponding to at least a “moderate” daily rainfall) belong to ST#1 and the relative percentage of ST#1 is then always  $<0.5\%$  for the WEs receiving  $\geq 22.35$ , 44.2 and 89 mm of rainfall.

It is clear that the largest RR of 3-hourly extreme rainfall is always observed for ST#2, especially in the central-northern part of the country and for heavy and very heavy rainfall (Figure 8c). The RR increases for ST#4 when the threshold of 3-hourly rain increases from 4 to 38.5 mm (Figure 8a–d). It is also interesting to note that the local RRs are usually anomalously lower than 1 for thresholds  $\geq 38.5$  mm/3 hr for ST#3 (Figure 8i) while the associated total amount is very close to the ST#2 one.

We then explore the probability of occurrence of a daily extreme  $\geq 9.65$ , 22.35, 44.2 and 89 mm during the four STs. When two different STs are observed on the same day and station, we consider only the ST accounting for the largest amount of rainfall as the “daily” ST. For ST#2, ST#3 and ST#4, RR is always significantly above 1 for the thresholds  $\geq 22.35$  and  $\geq 44.2$  mm but it is also very clear that RR decreases for ST#2 and ST#3 as daily amount increases (Figure 9). The RR becomes even significantly lower than 1 for ST#2  $\geq 89$  mm (Figure 9h). In contrast, the RR greatly increases for ST#4 with increasing daily amount (Figure 9m–p): for example,  $\sim 64\%$  of all daily amounts  $\geq 89$  mm are associated with ST#4 ( $\sim 21\%$  with ST#3 and  $\sim 13\%$  with ST#2). Figure 9e–p shows a rather coherent pattern with sometimes a difference between the southeastern part and the remainder of the country. It is also notable that the RR stays significant for some inner stations for ST#3 even for heavy and very heavy daily rain, while the RR is significantly lower to 1 in the southeast of the country for the same amount (Figure 9k,l).

This section basically shows that daily time scale emphasizes mostly the duration of the STs rather than their mean intensity, since the RR is especially enhanced for the longest ST (i.e., ST#4) and that the difference between ST#4 and ST#2 and ST#3 increases as the daily amount increases. It is rather expected that a longer WEs may lead to a potentially larger total amount at the end, but it does not say anything about the intra-WE intensity.

### 3.5 | Relationships between STs and intra-seasonal variability

The first intra-seasonal regional-scale mode is a northward propagating pattern of anomalous convection with a period of 30–60 days (usually referred to as boreal summer intra-seasonal oscillation [BSISO]) and found all across southern and equatorial Asia (Krishnamurthy and Shukla, 2000, 2007; Goswami and Ajayamohan, 2001; Lawrence and Webster, 2001; Moron *et al.*, 2012). This mode is related to the planetary-scale Madden–Julian oscillation (Singh *et al.*, 1992). A second mode of variation is referred to as the QBW mode of variation with a dominant E–W propagation across the whole southern Asian domain from the equatorial and tropical western North Pacific (Kikuchi and Wang, 2009; Hatsuzuka *et al.*, 2014; Hatsuzuka and Fujinami, 2017; Wang *et al.*, 2017; Sree Lekha *et al.*, 2020). We define a Bangladesh's OLR index (BOLR) as the spatial average of OLR over  $88^{\circ}$ – $92^{\circ}$ E and  $21^{\circ}$ – $25^{\circ}$ N. As an example, we show raw BOLR and its band-pass filtered variations for BSISO (25–60 days) and QBW (10–25 days) quasi-periodic oscillations in 1998–1999 in Figure 10. The main temporal variation is related to the annual cycle with a more abrupt winter-to-summer transition in 1999 than in 1998. BSISO (Figure 10b) and QBW (Figure 10c) variations are modulated across the annual cycle with usually a higher amplitude in boreal summer. BSISO and QBW convey respectively 14 and 31% of the intra-seasonal variance of BOLR over the 1998–2019 period. Sometimes, BSISO is more prominent than QBW as around March–April 1999 (Figure 10b) while QBW is more intense in most of the boreal summer of 1999 (Figure 10c).

The RR of each ST considering any 3-hourly slot when any WE occurs is evaluated for the 8 phases of BSISO and QBW BOLR index in the 1998–2019 period (Figures 11 and 12). As BOLR is a single country-side index at daily time scale, we first copied each daily phase eight times and then considered the same phase for the whole network of the 34 stations. Figure 11a,b shows the RR for the 34 stations considered all together respectively for QBW and BSISO. The phases 2 and 3 (black dashed curves in Figure 11a,b) correspond to negative OLR anomalies, thus usually to cyclonic low-level anomalies centered over Bangladesh. In contrast, the phases 6 and 7 correspond to positive OLR anomalies and anticyclonic low-level anomalies (Figure 11a,b). As expected from their contribution to the total intra-annual variance, the amplitude of QBW OLR anomalies is slightly larger than those related to BSISO. It is clear that the phase modulation of the ST#1 and ST#2 occurrence is reversed versus the one of ST#3 and ST#4 with the largest impact observed for ST#4 before ST#1 and the smallest one



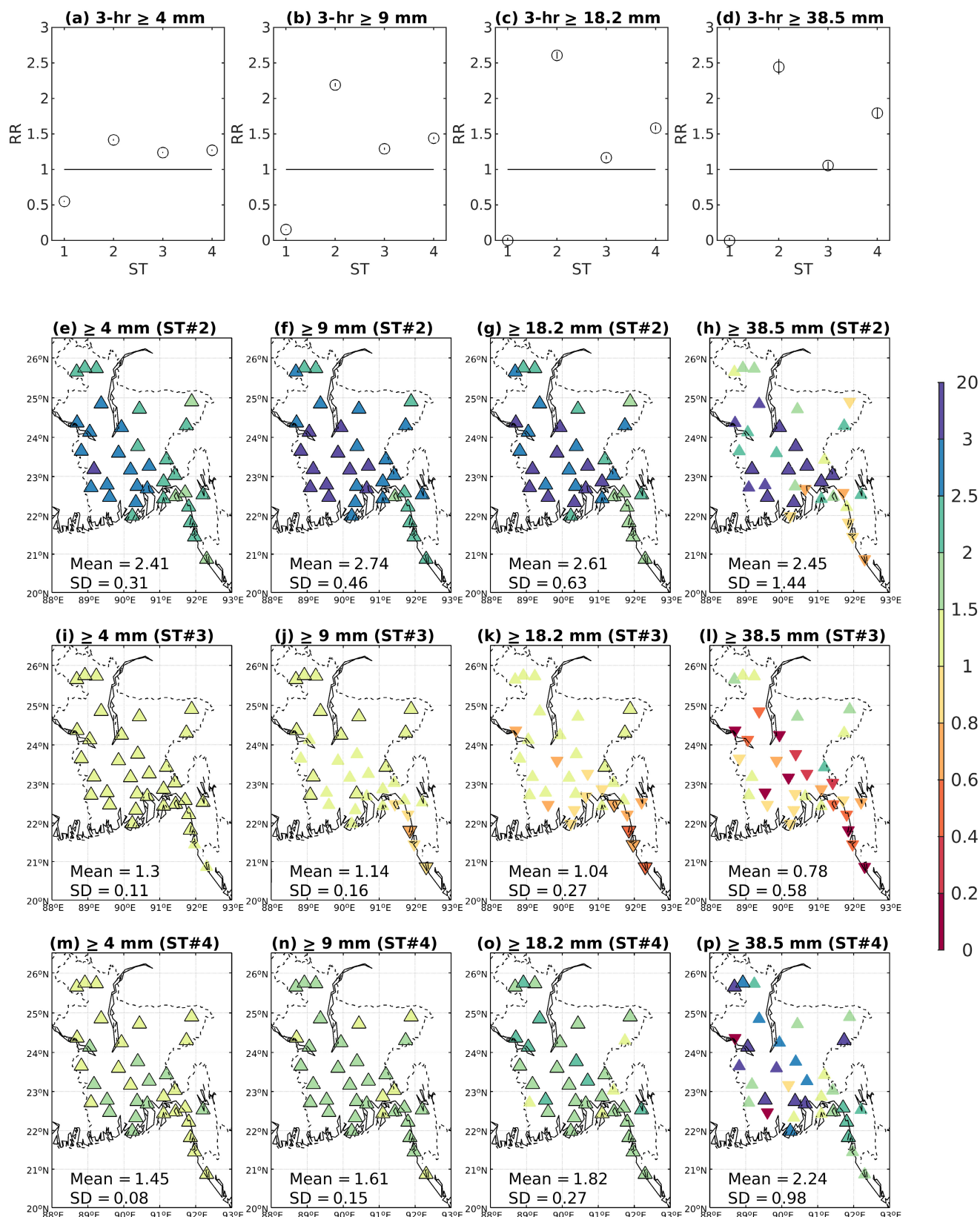


**FIGURE 8** (a–d) Relative RR (dots with vertical line showing the 99% confidence interval) of probability of occurrence in each ST across all stations of 3-hourly rain  $\geq 4$ , 9, 18.2 and 38.5 mm. The RR is computed by stations on panels (e–h) for ST#2, panels (i–l) for ST#3 and (m–p) for ST#4. The spatial average and SD of RR are indicated at the bottom of each panel. Contoured upward (for RR > 1) and downward (for RR < 1) triangles indicate anomalous significant RR at the 99% level [Colour figure can be viewed at [wileyonlinelibrary.com](http://wileyonlinelibrary.com)]

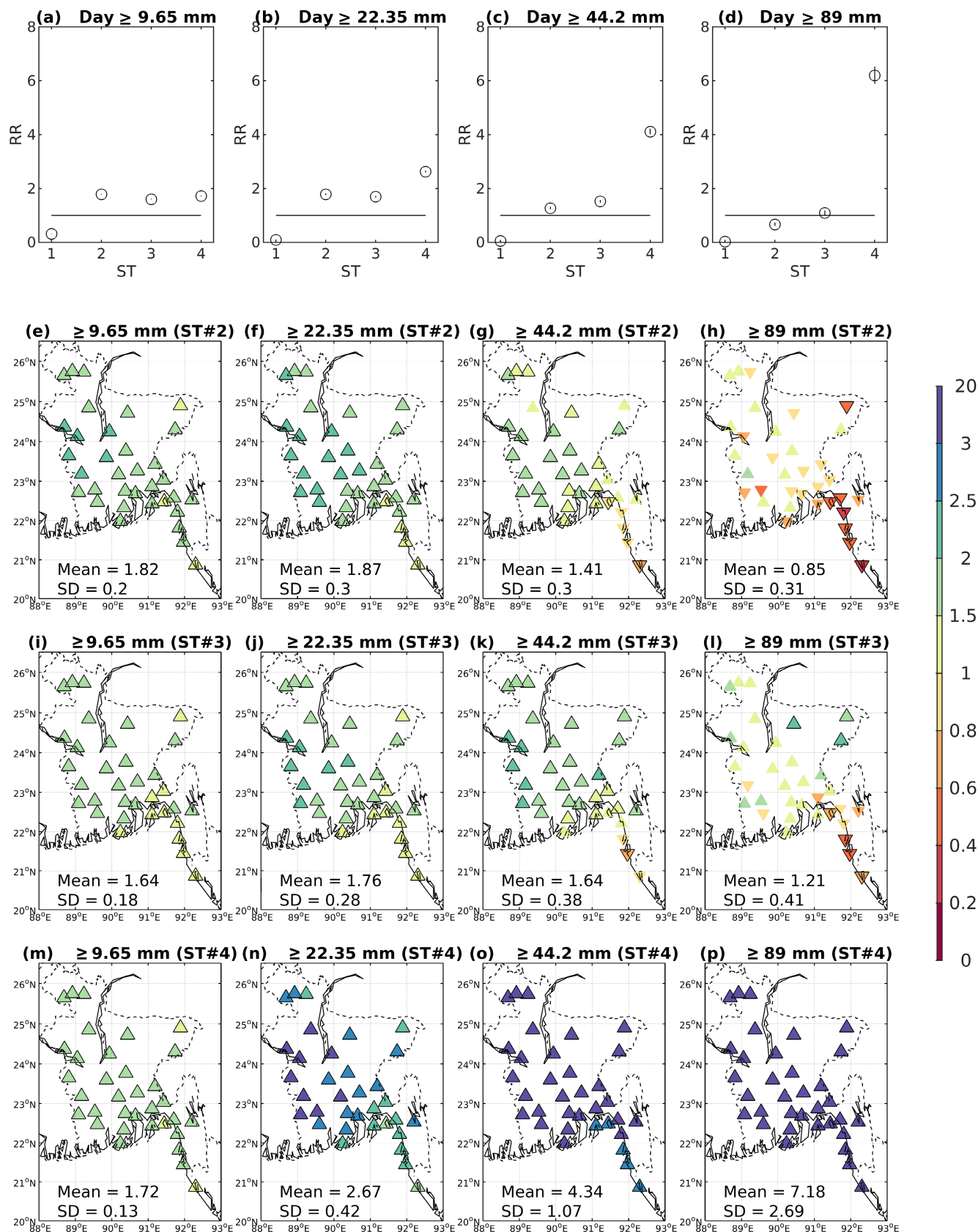


**FIGURE 9** Same as Figure 8 except for daily rainfall  $\geq 9.65$ , 22.35, 44.20 and 89 mm. These thresholds are used by BMD to define respectively moderate, heavy moderate, heavy and very heavy daily rainfall [Colour figure can be viewed at [wileyonlinelibrary.com](http://wileyonlinelibrary.com)]

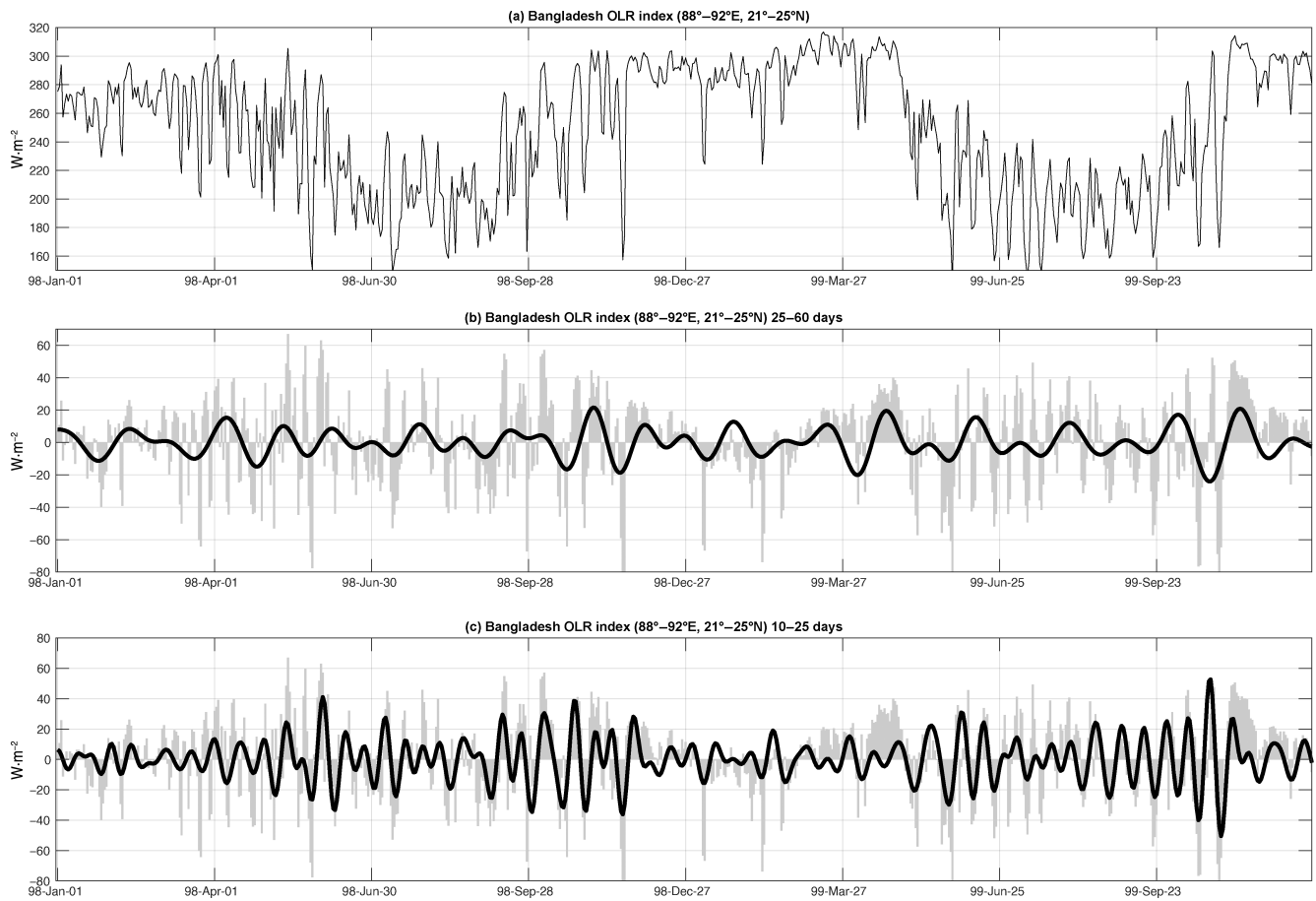


**FIGURE 10** (a) Example of the Bangladesh's OLR index (BOLR: spatial average of daily OLR over  $88^{\circ}$ – $92^{\circ}$ E,  $21^{\circ}$ – $25^{\circ}$ N) in 1998–1999 (in  $\text{W}\cdot\text{m}^{-2}$ ). Corresponding low-pass filtered intra-annual variations of BOLR faster than 180 days (grey bars) with band-pass filtered variations between (b) 25 and 60 days and (c) 10 and 25 days as black line (in  $\text{W}\cdot\text{m}^{-2}$ )

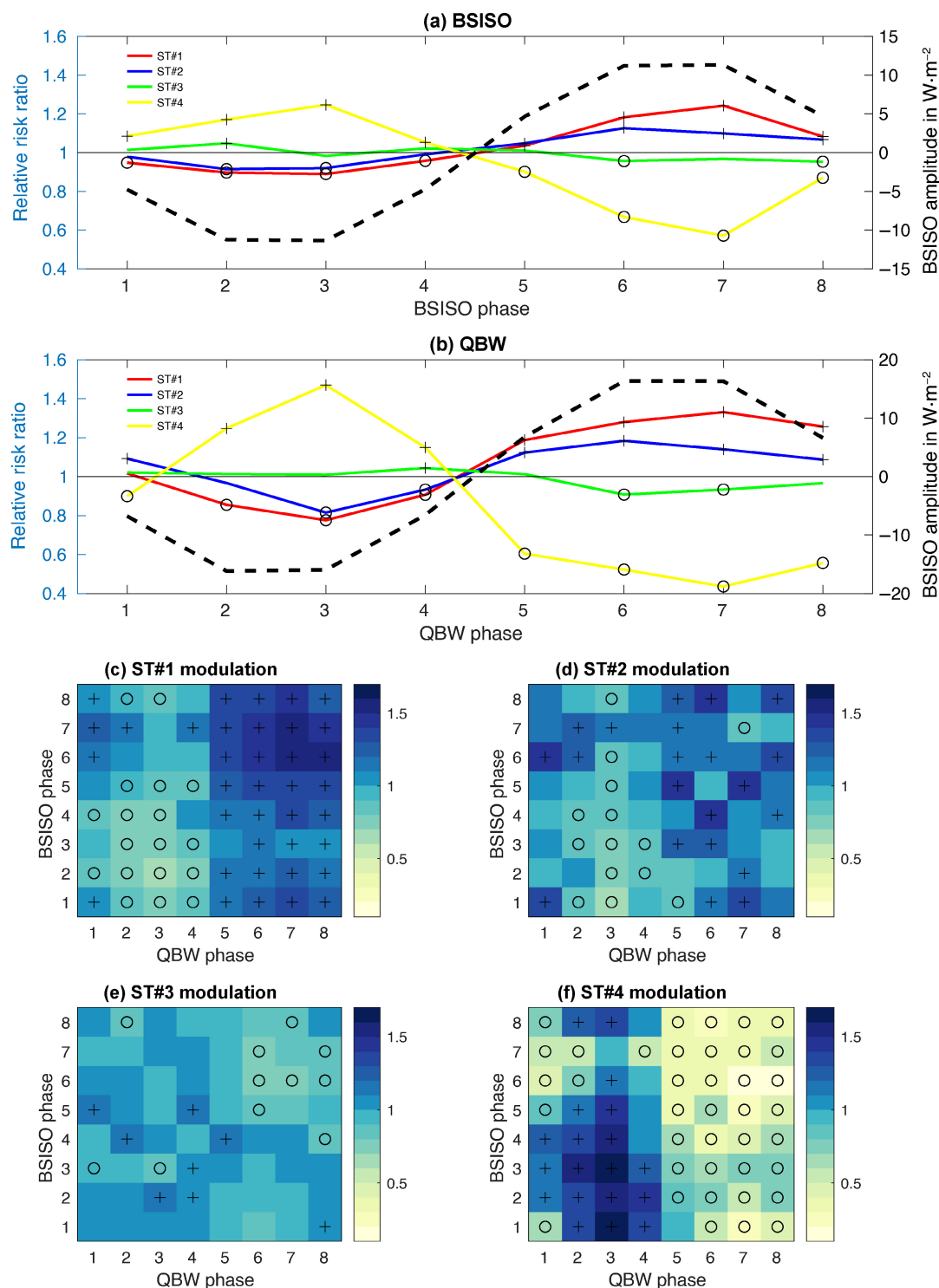
observed for ST#3. So, ST#1 and #2 occurrence is increased during positive OLR anomalies of both QBW and BSISO, while ST#4 occurrence is increased during negative OLR anomalies of them (Figure 11a,b). Figure 11c–f considers the conditional RR with QBW and BSISO modes of variation. It is rather clear that QBW dominates somehow the conditional modulation of STs since the RR varies more in columns (related to QBW phases) than in rows (related to BSISO phases), especially for ST#1 (Figure 11c) and ST#4 (Figure 11f). But there is also some interaction between QBW and BSISO especially for ST#4 where the highest (respectively lowest) RRs are observed when OLR anomalies related to both modes are negative (Phases 2 and 3) (respectively positive, Phases 6 and 7). This is also observed for ST#1 with a reversed polarity.

Figure 12 shows the local-scale RR for phases 2 and 3 and 6 and 7 of QBW. Note that the RRs for the same phases of BSISO are highly similar with a lower amplitude (not shown). As expected from Figure 11, the RRs are broadly reversed between ST#1 (Figure 12a–d) and ST#2 (Figure 12e–h) on one hand and ST#4 (Figure

12m–p) on the other hand while the modulation of ST#3 is rather weak (Figure 12i–l). Even if the RR anomalies versus ST#1 are usually spatially consistent across Bangladesh, there are some subtle variations. For example, the anomalously positive  $\text{RR} > 1$  for ST#1 and also ST#2 in phases 6 and 7 are especially clear in the interior of the country while the anomalously negative  $\text{RR} < 1$  in phases 2 and 3 is larger over E-SE of the country. The  $\text{RR} > 1$  ( $< 1$ ) of ST#4 in phase 3 (phases 6 and 7) is more widespread across the country (Figure 12m–p).

### 3.6 | Relationships between STs and lows

A last analysis is done between ST occurrence and the lows recorded by IMD. A first step was to compute the RR of the occurrence of any ST versus the distance of LPS. The analysis is made first across all the stations and with running distances of 500 km (0–500 km, then 100–600 km, etc. till 2,000–2,500 km). This is re-done also by



**FIGURE 11** (a,b) Marginal relative risk ratio (RR) of the probability of occurrence (left axis) of each storm type (ST) in the eight phases of boreal summer intra-seasonal oscillation (BSISO) and quasi biweekly oscillation (QBW) modes of variation defined in Figure 10b,c. The black dashed line is the mean amplitude of BSISO and QBW modes of variation in  $\text{W}\cdot\text{m}^{-2}$  (right axis), (c,f) conditional RR of the probability of occurrence of each ST in the eight QBW (columns) and BSISO (rows) phases. The “+” and “o” signs indicate significant positive and negative RR at the 99% level [Colour figure can be viewed at [wileyonlinelibrary.com](http://wileyonlinelibrary.com)]

splitting the LPS into two broad categories (depressions and cyclones). Figure 13a shows that the occurrence is increased for all STs till a distance of  $\sim 1,200$  km. The

modulation is strongest for ST#4 and weakest for ST#2 as for intra-seasonal variability, but it is of course possible to imagine a degree of redundancy between LPS and



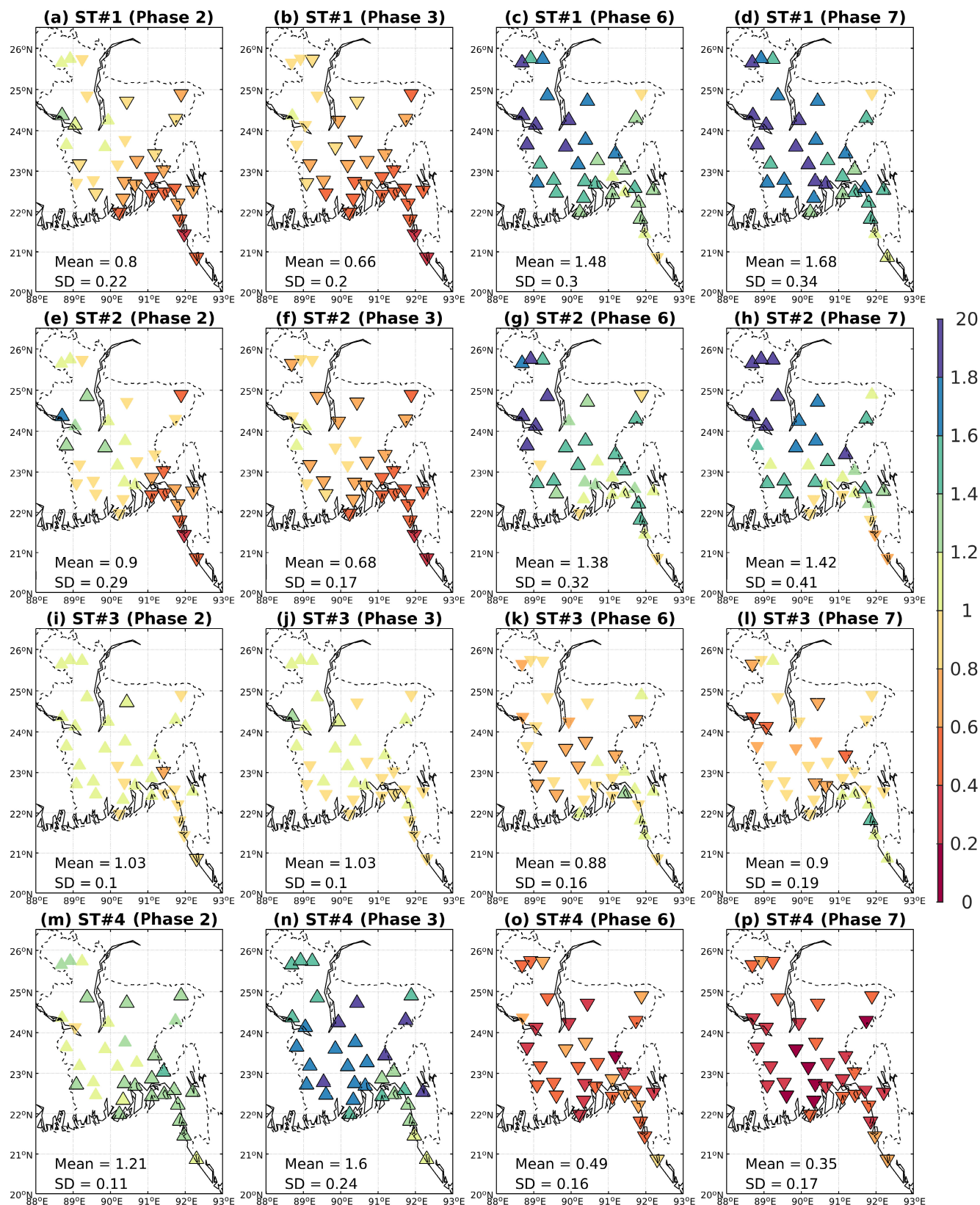


**FIGURE 12** Local relative RR of the probability of occurrence of each ST in the Phases 2 (a,e,i,m) and 3 (b,f,j,n) and 6 (c,g,k,o) and 7 (d,h,l,p) of QBW defined in Figure 10c. The contoured upward (for RR > 1) and downward (for RR < 1) triangles indicate significant RR at the 99% level of significance. The spatial average and SD are indicated at the bottom of each map [Colour figure can be viewed at [wileyonlinelibrary.com](http://wileyonlinelibrary.com)]

intra-seasonal variability considered in the previous section. The strength of the relationship decreases according to the increasing distances. Interestingly, the occurrence is usually significantly anomalously negative when LPS is further than 1,500 km. In this case, most of the LPS centres are in the Arabian Sea or close to the equator in the southern BoB. It is possible that anticyclonic regional-scale subsidence related to upper-level outflow >1,500 km from LPS centre then inhibits rainfall across Bangladesh. This relationship is strongest for cyclones than for weaker depressions (Figure 13b,c) except for ST#2 which is no longer significantly impacted at close distance (Figure 13c). Now, the RR of ST#4 in a 0–500 km radius from the cyclone centre is >18 times its occurrence when no LPS is recorded. What does it mean when we consider the relative frequency of STs? Respectively 11%, 8%, 12% and 22% of all ST#1, ST#2, ST#3 and

ST#4 occur when a LPS centre is less than 1,500 km from a BMD's stations. These relatively small proportions should be contextualized with the fact that such a distance to a LPS centre accounts for slightly less than 7% of the total 3-hourly available records across the 34 stations.

Figure 14 shows the local RR for a selection of four distances. At short distances  $\leq 500$  km, RRs are almost always significantly positive, except for ST#2 in the north (Figure 14a,e,i,m). Between 600 and 1,000 km, RRs are of course lower but still significant across the country especially for ST#1, ST#3 and ST#4 (Figure 14b,f,j,n). The RR decreases clearly, and becomes significantly negative between 1,000 and 1,500 km mostly in the north but also over the southern delta, especially for ST#1 and ST#3 (Figure 14c,g,k,o). At the farthest distance, the RR is positive only for ST#4, but with a different pattern than at short and medium distances, that is, mostly on the

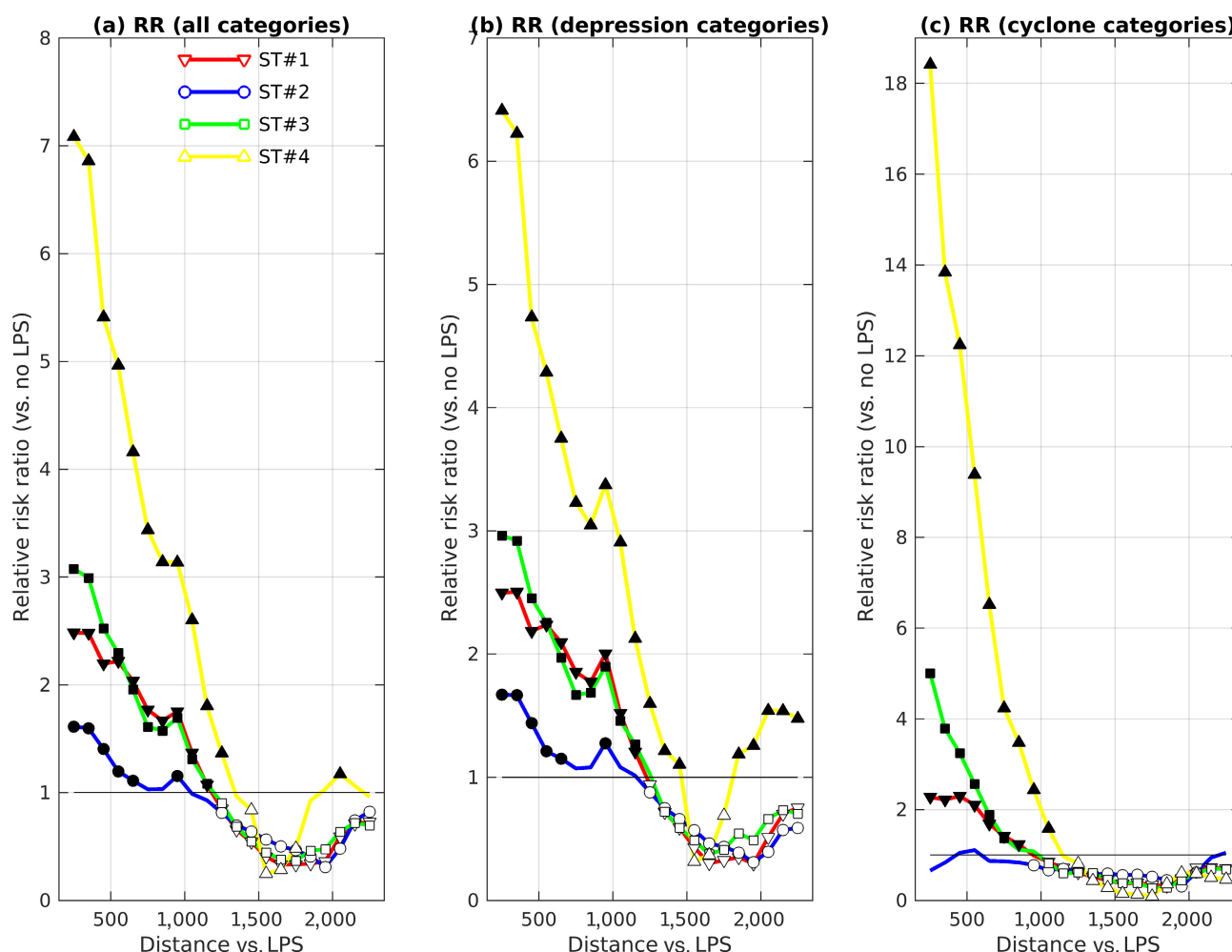


**FIGURE 13** Local relative RR of the probability of occurrence of any STs (markers defined in panel [a]) versus the distance from LPS (vs. no LPS) for (a) all LPS, (b) only depressions and (c) only cyclones. The distances are defined as running 500-km radius from 0–500 km to 2,000–2,500 km with a step of 100 km. Filled (unfilled) black markers show significant positive (negative) anomalous RR (vs. RR of 1) at the two-sided 99% level [Colour figure can be viewed at [wileyonlinelibrary.com](http://wileyonlinelibrary.com)]

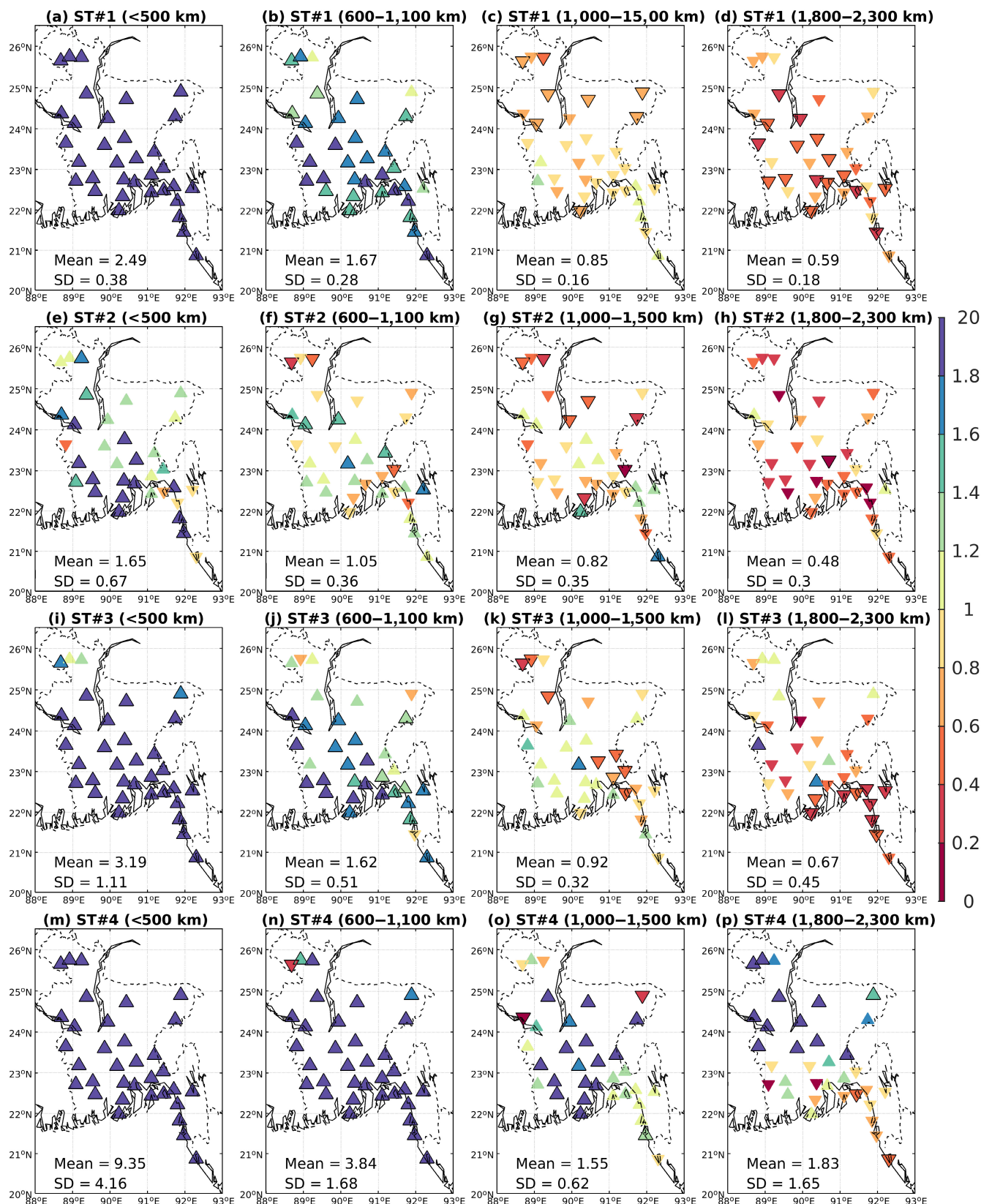


**FIGURE 14** Local relative RR of the probability occurrence of ST#1 to ST#4 when a LPS centre is (a,e,i,m) less than 500 km from BMD stations, (b,f,j,n) between 600 and 1,100 km from BMD stations, (c,g,k,o) between 1,000 and 1,500 km from BMD stations and (d,h,l,p) between 1800 and 2,300 km from BMD stations. The contoured upward (for  $RR > 1$ ) and downward (for  $RR < 1$ ) triangles indicates significant anomalous RR at the 99% level. The spatial average and SD are indicated at the bottom of each map [Colour figure can be viewed at [wileyonlinelibrary.com](http://wileyonlinelibrary.com)]



northern half of the country while the RRs are  $<1$  over the southern part (Figure 14p).

## 4 | DISCUSSION AND CONCLUSION

We explore the characteristics of total 96,190 WEs, defined as consecutive 3-hourly rainfall  $\geq 1$  mm, across a network of 34 stations across Bangladesh from 1998 to 2019. As demonstrated elsewhere (Deshpande *et al.*, 2012; Trenberth *et al.*, 2017; Moron *et al.*, 2021), most of the WEs are short and associated with a small total amount of rainfall (Figure 2). In particular, we found similar results to a previous study done over India (Moron *et al.*, 2021). Despite the longer time step used here (3-hr vs. 1-hr),  $\sim 80\%$  (respectively  $\sim 90\%$ ) of the WEs last 6 hr at maximum here and these WEs contribute to  $\sim 50\%$  (respectively  $\sim 60\%$ ) of the total amount of rainfall (respectively in India). The small difference could be simply due to the fact that Bangladesh is overall wetter than India in mean, and thus associated with longer wet spells (Trenberth *et al.*, 2017; Zhang and Wang, 2021). Inside Bangladesh, there is indeed a very strong positive relationship between mean duration of WEs and total rainfall (Figure 2) with longest/shortest WEs occurring over southeastern/central-western parts of the country (Figure 2). Despite different starting point, data and processing, it is also interesting to note that the average duration of the 96,190 WEs here ( $= 2.05$  3-hourly slots) is very close to the average lifetime of precipitation systems developed over Bangladesh and detected by a weather radar ( $= 5.7$  hr) (Islam *et al.*, 2005b).

The 96,190 WEs are dynamically clustered into four canonical STs. The use of a 3-hourly timestep does not allow to distinguish as many clusters as with a 1-hr timestep, since a lot of variations occur in the first few hours of the WEs. The method of normalization of 3-hourly local rainfall (considering the 3-hourly square-rooted anomalies relative to the average of each 3-hr slot referred to the starting time of each WE) leads to the fact that duration and intensity account for a fraction of the total variance, and are thus both considered in the clustering. It is interesting to note that duration and mean intensity are barely independent (Figure 4b). The total amount of rainfall during WEs could be viewed as a cross-product of duration and intensity. Figure 3b shows that duration is slightly better discretized than intensity by the STs.

As in India, a very short and nominal ST (ST#1) is, by far, the most frequent. It is associated with low intensity. Obviously, we cannot exclude the fact that, for these events especially, it does not rain all along the 3 hr and

then, the real intensity may be more or less strongly underestimated, since the total amount then falls in a duration shorter than three consecutive hours. But the fact that these STs account for a similar relative frequency as in India with a 1-hr resolution suggests that this potential bias is probably not so strong. Then, two STs (ST#2: very short and intense in mean; ST#3: short and not so intense in mean) rather similar from the point of view of the total rainfall amount, are mostly discretized by their intensity (Figure 4). A last rare ST (ST#4) is associated with long duration (usually  $\geq 15$  hr) and a large total amount of rainfall, while the mean intensity is slightly lower than the very short and intense ST#2 (Figure 4). The surface of wet areas (as seen in IMERG) is positively related to duration (Figures 6 and 7). It is fully expected since a large atmospheric rain-bearing system (meso-scale complex, tropical low, depression, cyclone, etc.) may lead to a relatively long local WE as soon as its speed is relatively low (Ricciardulli and Sardeshmukh, 2002; Zhang and Wang, 2021). If so, its quasi-stationarity in space leads to a WE as long as the system is over the rain gauge and a larger system leads logically to a longer duration.

Figures 4, 6 and 7 offer a synthetic view of the relationship between duration, intensity, total amount and area of WEs. It simply illustrates the ergodic nature of the climate system, involving in particular a tight link between the spatial and time scales of any atmospheric phenomena. For example, an isolated thunderstorm related to a single cumulo-nimbus will last far less and cover a smaller wet area than an organized and long-lasting LPS. Such distinct phenomena can be captured from either the duration of a local WE (Figure 4) or the contiguous wet area of a temporally aggregated rainfall field (Figures 6 and 7). These points of view are complementary in the sense that duration and wet areas are both able to discretize different space-time scales of atmospheric phenomena. In that context, we could view the duration as a pivotal characteristic: it is positively and largely related to both total amount (Figure 4) and area (Figure 7) of WEs. In consequence, total amount is also positively related to area, as already observed from daily rainfall across the whole tropical zone (Moron and Robertson, 2021). On the contrary, mean intensity is rather independent from duration, total amount as well as area of WEs. Again, mean intensity over a 3-hr timestep is not equivalent to the mean instantaneous rain rate as soon as the WE does not cover the whole 3-hr slot. It may be especially critical here for ST#1 and also ST#2. But, it still suggests that duration/area/total amount and intensity are two different (and here independent) characteristics of any tropical WE (Moron and Robertson, 2021). It remains to understand what are the



main drivers of both properties and their space–time variations across the year, and also at interannual time scale. It will be interesting to explore these relationships considering other tropical sectors, including some areas where the deep convection is not the main rain-bearing process and where warm stratiform clouds contribute to a large fraction of the total rainfall (as oceanic area over warm waters as well as equatorial wet sectors over forests). Figure 8 indicates that the relative risk ratios of 3-hourly “extremes” are emphasized mostly for ST#2, then for ST#4, while Figure 9 shows broadly that considering daily time scale greatly emphasizes the duration versus the mean intensity, since the RR of occurrence of a daily amount  $\geq$  given level increases the most for the longest ST (i.e., ST#4) and that this relative RR increases as the daily amount threshold increases. It suggests that considering daily rainfall will not offer an optimal discretization of mean intensity, which could have specific socio-economic consequences.

The association between STs and rain-bearing systems is probably complex at least because regional-scale rain-bearing systems (as lows to tropical cyclones) include of course smaller scale ones (as unitary cumulonimbus or meso-scale convective complex). We may hypothesize that a given WE is mostly faceted by the largest scale involved. For example, a WE lasting one day could not be an isolated thunderstorm and should be implied by a large-scale quasi-stationary or slowly travelling system or by the interaction between a mean flow and a fixed element of the geography (as a relief). But, we cannot exclude that a WE lasting less than 3 hr and leading to a small amount of rainfall at a local scale is in fact sometimes related to the external margins of a bigger system. Considering a large sample of events suggests that this potential effect does not crudely bias the analyses. If we assume these precautions, we can make several hypotheses about the main rain-bearing systems associated with each ST. ST#1, but also ST#2, may be related to scattered small-scale thunderstorms. ST#1 also includes some exotic and very rare longer WEs when the rainfall starts weakly but is followed by scattered peaks of rainfall (not shown). ST#2 is far more intense in mean than ST#1. It is indeed the most intense ST in mean (Figure 4). Interestingly, its relative frequency peaks in March–May during the pre-monsoon season (Figure 5e) and then secondly in October when the boreal summer monsoon retreats southward. ST#2 is also the ST which is least impacted by the synoptic lows/depressions defined by IMD (Figure 13). So, ST#2 may be related to small-scale processes favoured mostly before the main rainy season when the solar radiation is close to its maximum, weak southerlies already advect some low-level moisture across the country but when the soils are not

fully wetted by the monsoonal rains. Such conditions may promote a large building of CAPE and thus potentially very intense thunderstorms. But the dynamical atmospheric environment is probably not necessarily favourable to a large-scale organization of the deep convection. It is also intriguing that ST#1 and ST#2 occurrences are favoured during the phase of positive OLR anomalies related to QBW and BSISO modes of variations (Figures 10–12). If positive OLR anomalies are related to anticyclonic low-level anomalies, it may inhibit the organization of deep convection into regional-scale and long-lasting wet patterns, but also promote an intense warming able to trigger isolated, but possibly violent (as exemplified by ST#2) thunderstorms as soon as enough moisture is available. This hypothesis needs to analyse the atmospheric environment related to STs and will be explored in future studies.

ST#3 is characterized by larger and longer events than ST#2. The modulation by lows/depressions is also stronger than for ST#2 (Figures 13 and 14) but this ST is the least impacted by QBW and BSISO modes of variation. A median wet area covering  $10^5$  km<sup>2</sup> (Figure 7) is typically associated with large meso-scale convective complexes (Orlanski, 1975). This ST shows a rather constant relative modulation during the whole rainy season (Figure 5e). Lastly, ST#4 shows the strongest modulation due to either intra-seasonal variability modes (Singh *et al.*, 1992; Kikuchi and Wang, 2009; Hatsuzuka *et al.*, 2014) and lows/depressions (Goswami *et al.*, 2003). Despite this strong last impact, almost 80% of these ST#4 WEs are not related to any identified low/depression by IMD. Obviously, a larger frequency may be expected if the lows are specifically defined over Bangladesh (Hatsuzuka *et al.*, 2014; Hatsuzuka and Fujinami, 2017) but these lows are indeed smaller (i.e.,  $\sim 600$  km) than those defined for the whole Indian subcontinent by IMD. The largest impact of LPS over southeast Bangladesh (Figure 5d) suggests another process as the interaction between a southerly moist flow and the topography. Long and moderately intense rainfall may then occur windward of the orography stretched parallel to the coast and close to Myanmar's border. Further studies will explore the atmospheric environment of the ST#4.

Lastly, this approach gives some clues about the predictability issue since the potential predictability of seasonal amounts is considered to be moderate at best (Chowdhury and Ward, 2007; Hossain *et al.*, 2019; Kelley *et al.*, 2020; Acharya *et al.*, 2021). A poor predictability at interannual time scale may be related to various sources including intense and very localized rainy events (Stephenson *et al.*, 1999) and the lack or weakness of space–time organization of instantaneous rainfall by predictable regional to large scales (Moron and Robertson,

2021). Even a predictable signal at intra-seasonal time scale (BSISO and QBW here) is not necessarily beneficial to the interannual time scale if it leads to a near-zero residual at the end of the rainy season. Figures 11–14 suggest first that synoptic and intra-seasonal prediction may be more beneficial for ST#3 and especially ST#4 than for ST#2. Of course, it says nothing about the interannual predictability and more work is needed to estimate the role of regional-scale or planetary-scale mode of variations (as ENSO) on the probability of occurrence of each ST (Chowdhury, 2003; Islam *et al.*, 2021). About the consequences on the seasonal rainfall amount, its predictability may be decreased by at least three facts: first, ST#2 which is the least ST impacted by either intra-seasonal variability modes (Figures 11 and 12) and lows/depressions (Figures 13 and 14) contributes to nearly 30% of local-scale total rainfall. It is also the most intense ST in mean. So, this amount of rainfall may be interpreted as an unpredictable noise at any temporal scales, except when a low/depression is very close to Bangladesh and then increases the probability of occurrence of this ST, but as any ST (Figure 13). Second, ST#1, despite its small individual amount of rainfall, contributes to nearly 15% of local-scale total rainfall. Third, the intra-seasonal modulation of occurrence of STs by BSISO and QBW is reversed between ST#2 (and weakly ST#1) and ST#4 (and weakly ST#3). This last fact may even decrease the predictability of rainfall amount at intra-seasonal time scale. We must of course explore more deeply the possible systematic modulation of the occurrence of each ST due to boundary forcing at inter-annual scales, but the above result suggests that at least 45% of local-scale total rainfall may be not or poorly predictable at the synoptic and intra-seasonal time scales.

## AUTHOR CONTRIBUTIONS

S. M. Quamrul Hassan provided the 3-hourly rainfall data and checked for inconsistencies and errors. Vincent Moron designed the study, made the statistical analyses and produced the figures. Vincent Moron wrote the first draft. All authors contributed to the final draft and discussion of the results.

## ACKNOWLEDGEMENTS

The climate division of the Bangladesh Meteorological Department is warmly acknowledged for providing the 3-hourly data over the network of 34 stations. We thank both the reviewers for their constructive comments that improve a lot of readability of our paper.

## REFERENCES

Acharya, N., Mason, S.J. and Hassan, S.M.Q. (2021) On the next generation (NextGen) seasonal prediction system for Bangladesh. *Climate Prediction S&T Digest*, 33. [https://www.nws.noaa.gov/ost/STIClimateBulletin/CDPWDigest/45CDPW\\_Digest\\_IR.pdf](https://www.nws.noaa.gov/ost/STIClimateBulletin/CDPWDigest/45CDPW_Digest_IR.pdf)

- Ahmed, T., Hong, S.H., Jin, H.G., Lee, J. and Baik, J.J. (2021) Evaluation of IMERG data in Bangladesh and surrounding regions and their application to studying diurnal variation of precipitation. *Theoretical and Applied Climatology*, 146, 395–410.
- Ahmed, R. and Karmakar, S. (1993) Arrival and withdrawal dates of the summer monsoon in Bangladesh. *International Journal of Climatology*, 13, 727–740.
- Barbero, R., Fowler, H.J., Lenderink, G. and Blenkinsop, S. (2017) Is the intensification of precipitation extremes with global warming better detected at hourly than daily resolutions? *Geophysical Research Letters*, 44, 974–983.
- Basher, A., Stiller-Reeve, M.A., Saiful Islam, A.K.M. and Bremer, S. (2018) Assessing climatic trends of extreme rainfall indices over Northeast Bangladesh. *Theoretical and Applied Climatology*, 134, 441–452.
- Brammer, H. (2017) Bangladesh's diverse and complex physical geography: implications for agricultural development. *International Journal of Environmental Studies*, 74, 1–27.
- Chowdhury, M.R. (2003) The El Niño-Southern Oscillation (ENSO) and seasonal flooding – Bangladesh. *Theoretical and Applied Climatology*, 76, 105–124.
- Chowdhury, M.R. and Ward, M.N. (2007) Seasonal flooding in Bangladesh – variability and predictability? *Hydrological Processes*, 21, 335–347.
- Dastagir, M.R. (2015) Modeling recent climate change induced extreme events in Bangladesh: a review. *Weather and Climate Extremes*, 7, 49–60.
- Deshpande, N.R., Kulkarni, A. and Krishna Kumar, K. (2012) Characteristic features of hourly rainfall in India. *International Journal of Climatology*, 32, 1730–1744.
- Diday, E. and Simon, J.C. (1976) Clustering analysis. In: Fu, K.S. (Ed.) *Digital Pattern Recognition (Communication and Cybernetics)*, Vol. 10. Berlin: Springer, pp. 47–94.
- Gadgil, S. (2003) The Indian monsoon and its variability. *Annual Review Planetary Sciences*, 31, 429–467.
- Godbole, R.V. (1977) The composite structure of the monsoon depression. *Tellus*, 29, 25–40.
- Goswami, B.N. and Ajayamohan, R.S. (2001) Intraseasonal oscillations and interannual variability of the Indian summer monsoon. *Journal of Climate*, 14, 1180–1198.
- Goswami, B.N., Ajayamohan, R.S., Xavier, P.K. and Sengupta, D. (2003) Clustering of synoptic activity by Indian summer monsoon intraseasonal oscillations. *Geophysical Research Letters*, 30, 1431.
- Hatsuzuka, D. and Fujinami, H. (2017) Effects of the South Asian monsoon intraseasonal modes on genesis of low pressure systems over Bangladesh. *Journal of Climate*, 30, 2481–2499.
- Hatsuzuka, D., Yasunari, T. and Fujinami, H. (2014) Characteristics of low pressure systems associated with intraseasonal oscillation of rainfall over Bangladesh during boreal summer. *Monthly Weather Review*, 142, 4758–4774.
- Hossain, Z., Azad, A.K., Karmakar, S., Islam Mondal, M., Das, M., Rahman, M. and Haque, A. (2019) Assessment of better prediction of seasonal rainfall by climate predictability tool using global sea surface temperature in Bangladesh. *Asian Journal of Advanced Research and Reports*, 4, 1–13.
- Huffman, G.J., Bolvin, D.T., Braithwaite, D., Hsu, K., Joyce, R., Kidd, C., Nelkin, E.J., Sorooshian, S., Tan, J. and Xie, P. (2017)

- NASA Global Precipitation Measurement (GPM) Integrated Multi-Satellite Retrievals for GPM (IMERG). Algorithm Theoretical Basis Document (Version 4.6), 28 pp.
- Huffman GJ, Bolvin, D.T., Braithwaite, D., Hsu, K., Joyce, R., Kidd, C., Nelkin, E.J., Sorooshian, S., Tan, J. and Xie, P. (2019) Algorithm Theoretical Basis Document (ATBD) (Version 06). NASA Global Precipitation Measurement (GPM) Integrated Multi-Satellite Retrievals for GPM (IMERG). NASA. Available at: <https://gpm.nasa.gov/>
- Huffman, G.J., Bolvin, D.T., Nelkin, E.J. and Tan, J. (2020) Integrated Multi-satellite Retrievals for GPM (IMERG) technical documentation. NASA/GSFC. Available at: <https://gpm.nasa.gov/>
- Islam, A.R.M. (2018) Statistical comparison of satellite-retrieved precipitation products with rain gauge observations over Bangladesh. *International Journal of Remote Sensing*, 39, 2906–2936.
- Islam, M.N., Hayashi, T., Terao, T., Uyeda, H. and Kikuchi, K. (2005a) The characteristics of precipitation systems analyzed from radar data over Bangladesh. *Journal of Natural Disaster Science*, 27, 17–23.
- Islam, A.R.M., Rahman, S., Khatun, R. and Hu, Z. (2020) Spatio-temporal trends in the frequency of daily rainfall in Bangladesh during 1975–2017. *Theoretical and Applied Climatology*, 141, 869–887.
- Islam, A.R.M., Salam, R., Yeasmin, N., Kamruzzaman, M., Shahid, S., Fattah, A., Shanawaz Uddin, A.S.M., Shahariar, M. H., Mondol, A.H., Jhajharia, D. and Techato, K. (2021) Spatio-temporal distribution of drought and its possible associations with ENSO indices in Bangladesh. *Arabian Journal of Geosciences*, 14, 2681.
- Islam, M.N., Terao, T., Uyeda, H., Hayashi, T. and Kikuchi, K. (2005b) Spatial and temporal variations of precipitation in and around Bangladesh. *Journal of Meteorological Society of Japan*, 83, 23–41.
- Islam, M.N. and Uyeda, H. (2007) Use of TRMM in determining the climatic characteristics of rainfall over Bangladesh. *Remote Sensing of Environment*, 108, 264–276.
- Kelley, C., Acharya, N., Montes, C., Krupnik, T.J., Abdul Mannan, M. and Quamrul Hassan, S.M. (2020) Exploring the predictability of within-season rainfall statistics of the Bangladesh monsoon using North American multimodel ensemble outputs. *Theoretical and Applied Climatology*, 141, 495–508.
- Kikuchi, K. and Wang, B. (2009) Global perspective of the quasi-biweekly oscillation. *Journal of Climate*, 22, 1340–1359.
- Krishnamurthy, V. and Shukla, J. (2000) Intraseasonal and interannual variability of rainfall over India. *Journal of Climate*, 13, 4366–4377.
- Krishnamurthy, V. and Shukla, J. (2007) Intraseasonal and seasonally persisting patterns of Indian monsoon rainfall. *Journal of Climate*, 20, 3–20.
- Lawrence, D.M. and Webster, P.J. (2001) Interannual variations of the intraseasonal oscillation in the South Asian summer monsoon. *Journal of Climate*, 14, 2910–2922.
- Liebmann, B. and Smith, C.A. (1996) Description of a complete (interpolated) outgoing longwave radiation data set. *Bulletin of American Meteorological Society*, 77, 1275–1277.
- Michelangeli, P.A., Legras, R. and Vautard, B. (1995) Weather regimes: recurrence and quasi stationarity. *Journal of Atmospheric Sciences*, 52, 1237–1256.
- Montes, C., Acharya, N., Hassan, S.M.Q. and Krupnik, T.J. (2021) Intense precipitation events during the monsoon season in Bangladesh as captured by satellite-based products. *Journal of Hydrometeorology*, 22, 1405–1419.
- Mooley, D.A. (1973) Some aspects of Indian monsoon depressions and the associated rainfall. *Monthly Weather Review*, 101, 271–280.
- Moron, V., Barbero, R., Fowler, H.J. and Mishra, V. (2021) Storm types in India: linking rainfall duration, spatial extent and intensity. *Philosophical Transactions of the Royal Society A*, 379, A20200137.
- Moron, V. and Robertson, A.W. (2021) Relationships between subseasonal-to-seasonal predictability and spatial scales in tropical rainfall. *International Journal of Climatology*, 41, 5596–5624.
- Moron, V., Robertson, A.W. and Ghil, M. (2012) Impact of the modulated annual cycle and intraseasonal oscillation on daily-to-interannual rainfall variability across monsoonal India. *Climate Dynamics*, 38, 2409–2435.
- Moron, V., Robertson, A.W., Ward, M.N. and Camberlin, P. (2007) Spatial coherence of tropical rainfall at the regional scale. *Journal of Climate*, 20, 5244–5263.
- Orlanski, I. (1975) A rationale subdivision of scales for atmospheric processes. *Bulletin American Meteorological Society*, 56, 527–530.
- Rafiuddin, M., Uyeda, H. and Islam, M.N. (2007) Characteristics of monsoon precipitation systems in Bangladesh during 2000–2005. In: *6th International Conference on Mesoscale Meteorology and Typhoon in East Asia (ICMCS-VI)*.
- Rafiuddin, M., Uyeda, H. and Islam, M.N. (2010) Characteristics of monsoon precipitation systems in and around Bangladesh. *International Journal of Climatology*, 30, 1042–1055.
- Ricciardulli, L. and Sardeshmukh, P. (2002) Local time- and space scales of organized tropical deep convection. *Journal of Climate*, 15, 2775–2790.
- Rimi, R., Haustein, K., Barbour, E.J. and Allen, M.R. (2019) Risks of pre-monsoon extreme rainfall events of Bangladesh: is anthropogenic climate change playing a role? *Bulletin American Meteorological Society*, 100, S61–S65.
- Roller, C.D., Qian, J.H., Agel, L., Barlow, M. and Moron, V. (2016) Winter weather regimes in the northeast United States. *Journal of Climate*, 29, 2963–2979.
- Sabeerali, C.T., Sreejith, O.P., Acharya, N., Surendran, D.E. and Pai, D.S. (2022) Seasonal forecasting of tropical cyclones over the bay of Bengal using a hybrid statistical/dynamical model. *International Journal of Climatology* (in press). <https://doi.org/10.1002/joc.7651>
- Sattar, A.M. and Cheung, K.K.W. (2019) Comparison between the active tropical cyclone seasons over the Arabian Sea and Bay of Bengal. *International Journal of Climatology*, 39, 5486–5502.
- Shahid, S. (2011) Trends in extreme rainfall events of Bangladesh. *Theoretical and Applied Climatology*, 104, 489–499.
- Shahid, S. and Khairulmaini, O.S. (2009) Spatio-temporal variability of rainfall over Bangladesh during the time period 1969–2003. *Asia-Pacific Journal of Atmospheric Sciences*, 45, 375–389.
- Sikka, D.R. (1978) Some aspects of the life history, structure and movement of monsoon depressions. In: *Contributions to Current Research in Geophysics (CCRG)*. Basel: Birkhäuser. [https://doi.org/10.1007/978-3-0348-5759-8\\_21](https://doi.org/10.1007/978-3-0348-5759-8_21).

- Singh, S.V., Kripilani, R.H. and Sikka, D.R. (1992) Interannual variability of the Madden-Julian oscillations in Indian summer monsoon rainfall. *Journal of Climate*, 5, 973–976.
- Sree Lekha, J., Lucas, A.J., Sukhatme, J., Joseph, J.K., Ravichandran, M., Suresh Kumar, N., Thomas Farrar, J. and Sengupta, D. (2020) Quasi-biweekly mode of the Asian summer monsoon revealed in Bay of Bengal surface observations. *Journal of Geophysical Research: Oceans*, 125, e2020JC016271.
- Stephenson, D.B., Kumar, K.R., Doblas-Reyes, F.J., Royer, J.F., Chauvin, F. and Pezzulli, S. (1999) Extreme daily rainfall events and their impact on ensemble forecasts of the Indian monsoon. *Monthly Weather Review*, 127, 1954–1966.
- Trenberth, K.E., Zhang, Y. and Gehne, M. (2017) Intermittency in precipitation: duration, frequency, intensity, and amounts using hourly data. *Journal of Hydrometeorology*, 18, 1393–1412.
- Wang, B. and LinHo. (2002) Rainy season of the Asian–Pacific summer monsoon. *Journal of Climate*, 15, 386–398.
- Wang, M., Wang, J. and Duan, A. (2017) Propagation and mechanisms of the quasi-biweekly oscillation over the Asian summer monsoon region. *Journal of Meteorological Research*, 31, 321–335.
- Zhang, Y. and Wang, K. (2021) Global precipitation system size. *Environmental Research Letters*, 16, 054005.

**How to cite this article:** Moron, V., Acharya, N., & Hassan, S. M. Q. (2023). Storm types in Bangladesh: duration, intensity and area of intra-daily wet events. *International Journal of Climatology*, 43(2), 850–873. <https://doi.org/10.1002/joc.7835>